The Correlation of Electrochemical and Magnetic Techniques for use in Characterization of Underfilm Corrosion

by

Suzanne L. Wallace

B.S., Johns Hopkins University (1997)

Submitted to the Department of Materials Science and Engineering
in partial fulfillment of the requirements for the degree of

Master of Science in Materials Science and Engineering

at the

MASSACHUSETTS INSTITUTE OF TECHNOLOGY

June 1999

Author .....
Department of Materials Science and Engineering
May 07, 1999

Certified by .....
Professor Ronald M. Latanision
Director, H. H. Uhlig Corrosion Lab
Thesis Supervisor

Accepted by .....
Linn W. Hobbs, John F. Elliott Professor of Materials
Chairman, Departmental Committee on Graduate Students

The Correlation of Electrochemical and Magnetic Techniques for use in Characterization of Underfilm Corrosion

by

Suzanne L. Wallace

Submitted to the Department of Materials Science and Engineering
on May 07, 1999, in partial fulfillment of the
requirements for the degree of
Master of Science in Materials Science and Engineering

Abstract

Coated systems are used in many different applications. These systems, while less susceptible to corrosion than uncoated systems, are not impervious to corrosion. Since there is a coating, however, the traditional corrosion measurement techniques can not be used. Techniques such as electrochemical impedance spectroscopy (EIS) have been applied in this capacity. While EIS is useful in monitoring the degradation of the system, it has not previously been possible to definitively show a correlation between corrosion rate and mass loss data.

To quantify the mass loss and corrosion rate, an established technique from another discipline was used. The vibrating sample magnetometer (VSM) records the magnetic moment of a sample and the corresponding applied field. The magnetic saturation of a ferromagnetic material is a structure insensitive material property; thus it only changes with a change in mass and/or volume of a material. When a material is corroded it loses mass, and this mass change is detectable with a VSM.

The goal is to use the magnetic technique in conjunction with the electrochemical technique to determine mass loss and corrosion rate for a coated system. The groundwork for this was laid here. First the mass loss determined from gravimetric, electrochemical, and magnetic methods was correlated. This indicates that the methodology is possible. Next, the comparison between VSM and EIS data is necessary.

Before coated samples were used, bare cobalt foils and silicon wafers with sputter deposited cobalt were tested. The results of electrochemical and magnetic testing revealed a 1:1 relationship between the percent change in mass and the percent change in magnetic saturation. Samples were then coated with either an acrylic or a polyimide and were then tested using electrochemical impedance spectroscopy.

Thesis Supervisor: Professor Ronald M. Latanision
Title: Director, H. H. Uhlig Corrosion Lab

Acknowledgments

This research was supported by an NSF grant for the study of the fundamental aspects of underfilm corrosion. It was an international collaboration of some great people from three different countries. My gratitude is owed to these people: Prof. Ron Latanision and Dr. Bryce Mitton of MIT, Prof. George Thompson of UMIST in England, and Prof. Francesco Bellucci and Mr. Luca DeRosa of the University of Naples in Italy.

I would not have made it around the lab without the help of the wonderful group of people assembled in the H.H. Uhlig Corrosion Lab. First I owe my advisor, Prof. Latanision, for the opportunity to take part in this project. Bryce knows how much I owe him for everything. Dr. Gary Leisk and soon-to-be-Dr. Jason Cline were the best and most helpful office mates I could have had. Dr. Geetha Berera, Dr. Jae-Hong Yoon, Dr. Young-Sik Kim, and Dr. Seisho Take were always there to support me. Ellie Bonsaint made the administrative side of things easier. Although we started working together late in this project, Amy Lin was a great UROP. And I am grateful that what was started here will be continued by Nicolas Cantini, and of course, Bryce.

This thesis would never have been completed without the support and force of some helpful guys. I am quite glad that Sean George and Jason convinced me that LaTeXwas the way to go when writing my thesis, it was much smoother than I anticipated. Whenever I had questions while working on Athena, Alex Budge was always there to patiently answer them. I can not imagine how to express my gratitude to Sean and Gary for their assistance with assembling my thesis seminar transparencies.

As always, I must thank the people who supported my decision to pursue a graduate degree, and all of my decisions; my parents John and Linda Wallace, and my sister, Shannon. And finally, thanks to Sean for being there over these past two years when I've fallen apart and when I've succeeded.

Contents

List of Figures

List of Tables

Chapter 1

Introduction

Corrosion is a problem that has always affected mankind, and while it can currently be controlled to some extent, it will likely always exist. Each year it costs the US about $30 billion [1] in maintenance, repairs, and lost production time. A large part of that cost could be saved by utilizing the methods of protection and prevention available.

The protection and prevention methods available today consist of three main categories: materials selection and design, cathodic and anodic protection, and coatings [1]. Materials selection and design is the easiest to employ, since it should be a fundamental part of any engineering project. Cathodic and anodic protection involve either actively polarizing a system or employing a sacrificial system in connection with the main one. The third, coatings, finds widespread use in many different industries, such as microelectronics, automotive, infrastructure and construction, and food packaging. The primary function of these coatings is to act as a physical and chemical barrier between the corrosive environment and the structure being protected [2]. These coatings are not permanent solutions to corrosion issues, however. With time they can degrade through mechanical or chemical attack, and when the coating is compromised, corrosion begins to occur at the coating/metal interface. This corrosion beneath the coating is termed underfilm corrosion.

While it is known that underfilm corrosion takes place, and it can currently be detected visually after it has begun, and monitored electrochemically; there is much

yet to be learned on this subject. One problem of coated systems is delamination of the polymer. It is not known whether this delamination is due to a simple loss of adhesion or due to corrosion reactions and products at the interface. Methods are available to detect the existence of corrosion as well as the existence of delamination; however, currently there is not an exact technique to determine if the delamination was due to loss of adhesion from the swelling polymer and water aggregation or due to the corrosion occuring at the interface.

Techniques such as Electrochemical Impedance Spectroscopy (EIS) monitor the underfilm corrosion [3], but EIS can do no more than estimate the corrosion rate. Traditional corrosion testing methods which yield corrosion rates, involve knowledge of the mass loss of the material. Most simply, this can be done by weighing the sample before and after corrosion. A problem with coated systems is that an accurate mass loss measurement is difficult to make. The coating can swell when introduced to an electrolyte and it can trap corrosion products, causing inaccurate mass measurements. For non-coated, or bare metal samples, the relationship between the electrochemical data and the mass loss is well established in the literature [4] [2]. But for coated systems, this has not yet been satisfactorily achieved.

To establish a relationship between electrochemistry and mass loss of a coated system, a different approach to measuring mass loss had to be found. Certain metals known as ferromagnets exhibit a material property called magnetic saturation, (M_s). Saturation can be measured as an absolute value that is a known quantity when normalized by sample mass and volume [5]. Thus saturation is affected only by the amount of magnetic material. The change in the relative saturation can be used to indicate change in mass and volume of the metal [6]. It is possible to use a change in saturation to determine the corrosion rate by correlating the change in saturation and mass loss. The saturation measurements are not significantly affected by the polymer nor by non-ferromagnetic oxides present as corrosion products. Another potential benefit of employing magnetic measurements is that it should be possible to differentiate between delamination due to loss of adhesion or corrosion. Thus, only delamination due to corrosion can be detected by magnetic testing because only in

this case will there be a loss of magnetic material.

The study performed here used magnetic methods to correlate mass loss and electrochemical data for both a polymer coated metal and a non-coated metal. The next chapter will briefly explain the background of the corrosion principles employed here as well as the experimental setup and results of the electrochemical testing. Chapter 3 will do the same for the magnetics aspect of the project. The ensuing chapters will correlate the corrosion and magnetics results, the ultimate goal of this work.

Chapter 2

Corrosion

2.1 Background

Corrosion is a chemical reaction that occurs between a material and its environment. This is usually considered a destructive reaction that results in a loss of the material. Metallic corrosion involves charge transfer as the result of an oxidation reaction and a reduction reaction. The common anodic reaction is

$$M \leftrightarrow M^{n+} + ne^{-}$$

The corresponding cathodic reaction in an aqueous media is frequently one of the following:

$$2H^{+} + 2e^{-} \leftrightarrow H_2(g)$$

$$O_2 + 2H_2O + 4e^{-} \leftrightarrow 4OH^{-}$$

Water dissociation, which is essentially equivalent to the hydrogen reduction reaction, can also occur

$$2H_2O + 2e^{-} \leftrightarrow H_2(g) + 2OH^{-}$$

Determination of the reaction kinetics is important, it yields information about corrosion rates. The rate of electron charge transfer gives a good measure of the

reaction rates of corrosion. The current density, defined as the current (electron flow) per surface area, is proportional to the corrosion rate. Along with a current, there is a corresponding potential in the electrochemical cell which is a corroding metal.

A steady state potential known as the corrosion potential, E_{corr}, defines where the system is in an equilibrium with respect to the exchange of electrons due to the anodic and cathodic reactions. As the system's potential fluctuates from E_{corr} the potential change is referred to as polarization, or over-potential.

Another useful tool in studying corrosion is a quantity known as the Tafel constant. This constant relates polarization and current density. This is represented by the equation

$$\eta = \beta \log \frac{i}{i_o} \tag{2.1}$$

where η is the polarization, β is the Tafel constant, and i is the current density. The Tafel constant is usually in units of volts per decade. When the potential is plotted as a function of the log of the current density, the Tafel region, where this relationship holds, is a linear portion of the curve near the corrosion potential. This Tafel zone exists for both the cathodic and anodic reactions, and, in addition there are different corresponding constants for the two reactions.

2.2 Underfilm Corrosion

In a coated system, the degradation of the coated metal is governed by the same general corrosion reactions stated above, the difference is the protection provided by the coating. Thus, the entire corrosion process is not governed only by the electrolyte solution and the metal interactions, but also by the behavior of the organic coating.

For a polymer system to provide long-term protection, it must demonstrate strong mechanical resistance and adhesion, chemical stability, and low permeability [7]. The mechanical resistance and adhesion reflect the strength of the bond between the coating and the metal substrate. The coated system might be subjected to various loads in the working environment, and the coating should be able to withstand them. Chemical stability refers to the ability of the coating to maintain integrity during

chemical attack from such things as water, radiation, temperature, and different salts and ions. Permeability reflects the water or solution uptake of the coating. The lower the permeability of the coating to moisture, the lower is the probability that the substrate will encounter that environment.

There are two main mechanisms involved in protection by coatings, barrier behavior and reactions due to additives in the coating [8] [9]. As a barrier, the coating limits diffusion of water, oxygen, ionic species, and other corrosive agents. No coating is ever impermeable to these compounds, but the amount a coating limits permeation is a function of its capability to protect the substrate [10]. In resisting transport through the coating, it is also necessary to resist the transport laterally along the metal/coating interface. The additives in a coating can passivate the metal substrate, behave as an inhibitor to corrosion, or provide cathodic protection.

A coating will not function as a very good barrier if it is compromised. Thus the application of the film is often the limiting step in the performance of a coating [11]. A poor application can result in defects such as uneven regions, pinholes, cracks or crazes, local uncured zones, and nonuniform cross-linking. Since underfilm corrosion is usually a local event, even such small defects may initiate substrate degradation. A key factor in determining performance is the quality of the bond between the metal and the polymer. Often the bond is not with the metal itself, but with the native oxide film that has formed on the metal's surface [12]. The surface finish of the substrate is also quite relevant to the bond formed. Generally, smooth surfaces are considered to be superior since a polymer applied in the liquid form can achieve good contact. When the surface is rough, polymer penetration into the various topography depends on contact angle and pore shape of the surface, as well as the viscosity and flow properties of the polymer [13]. A good bond requires extensive molecular contact, which is affected by the surface energies and contact angles of the substrate and polymer. Organic polymers generally exhibit low contact angles on high energy substrates, but surface contaminations would lower these energies. Roughness does limit the contact with the polymer, but with a low contact angle and a low viscosity, an extended time before the cure or set can allow for a good bond [13]. One benefit

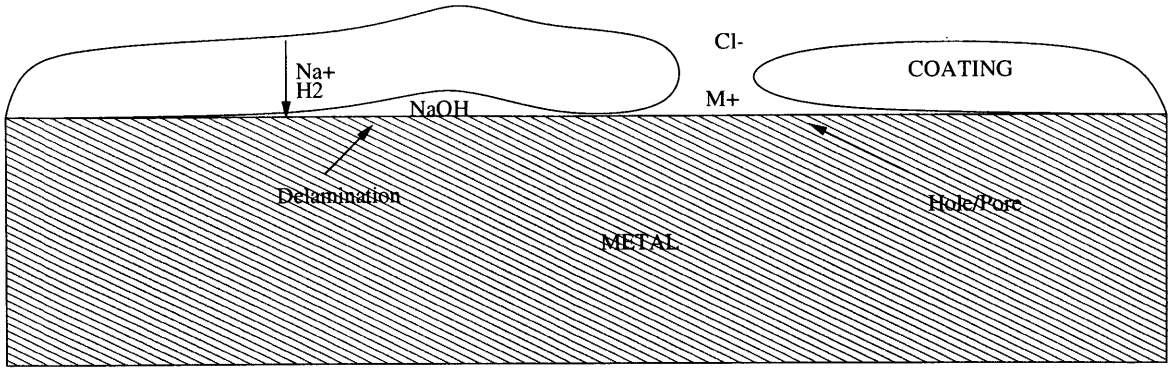

Figure 2-1: Schematic Cross Section of Underfilm Corrosion

of surface roughness is that it can alter the stress distribution of the surface, which can enhance bonds. Once a polymer is actually in use, however, the maintenance of a minimum level of adhesion is much more important than the initial bond strength [14].

Another common mode of coating failure is delamination [15] [8] [9]. This can occur due to a number of different processes. One can be poor wet adhesion, the aggregation of water at the polymer/metal interface weakens the adherence of the coating to the substrate. Another potential cause is cathodic delamination. The cathodic corrosion reaction, the oxygen reduction, creates a high pH environment which leads to delamination. The coating can also delaminate when the polymer swells due to uptake of the electrolyte solution. A schematic of delamination as a mode of underfilm corrosion can be seen in Figure 2-1. This shows a region of delamination occurring and a region where it has already occurred due to a defect such as a pore or hole or anything that allows the substrate and the solution to be in free contact and free ion exchange. In the region marked delamination there is an alkaline environment shown, the result of the cathodic corrosion reaction.

As in corrosion in the absence of a coating, corrosion underneath a polymer requires cathodic and anodic reactions. The reacting species need to migrate to the polymer/metal interface. This migration takes place through a few different methods. These pathways include activated diffusion, nonactivated diffusion, and interfacial

diffusion [8]. The nonactivated, or passive diffusion takes place through defects in a coating such as pores and pinholes. The uptake of water and ionic species is related to the diffusivity of the species in the organic medium, or the permeability of that medium. Migration of ions can also occur due to a gradient that is set up in the system, the coating/environment interface has one concentration of species or charge while the coating/metal interface has another, thus driving the electrolytes along the gradient. Interfacial diffusion occurs when there is already some water or solution aggregated at the metal/coating interface. The diffusion then occurs laterally along the interface. The migration of these ions may lead not only to corrosion but also to blistering of the coating and delamination [7]. This blistering is seen in regions where ionic conduction through the coating is enhanced.

2.3 Polymeric Coatings

Coatings can consist of many types of materials such as organic polymers, ceramics, or metallics [2]; however, polymers make up a majority of the coatings in use. Two specific coatings are of interest here. A polyimide coating is commonly used in microelectronics and an acrylic coating is used in the automotive industry.

2.3.1 Polyimides

Polyimides are formed through a two step process. The first step synthesizes polyamic acid from an aromatic diamine with pyromellitic dianhydride [16]. This is then applied to a substrate. The second step consists of heating the system between 200 and 400 ^{o}C to produce the polyimide. This process is an imidization reaction which releases water as a by-product. During this process an interaction between the polyamic acid and the metal substrate, or surface oxide, may occur which leads to chemical bonding and results in good adhesion [17]. This reaction is substrate dependent, however, and in some cases an adhesion promoter must be used.

In the field of semiconductor devices these polymers are used in two main roles: protection and interlayer dielectrics. As a protective polymer, polyimides are ap-

plied as junction coatings, buffer coatings, α-ray shielding, and in passivation roles. The advantages to using polyimides in this field are many—heat and chemical resistance, low dielectric constant, low temperature processing, elasticity, and absorption of mechanical stress. The disadvantages are lower thermal stability than some other polymer options, and high moisture absorption and penetration [18].

Polyimides have frequently been the study of underfilm corrosion research [19] [20] as the area of microelectronics is particularly sensitive to this form of corrosion. The amount of metal used in semiconductor devices is so minute that once initiated, corrosion can quickly destroy it. An example of a problem region is in the inner layers of a multi-layered microelectronic structure. This structure is composed of many alternating layers of dielectrics and metals, often more than one type of metal. These layers corrode more quickly than the outer layers because of the increased number of interfaces with different materials. Utilizing polyimides in these devices has brought about a decrease in this problem [18].

2.3.2 Acrylics

The type of acrylic used during this research project is a thermoset resin. These resins react chemically after they are applied. They contain functional groups that can react with different functional polymers or cross-linkers. A common functional polymer is a melamine-formaldehyde (MF). The acrylic is prepared by a free radical initiated chain-growth polymerization. This is cross-linked with a polymer, such as MF, resulting in ether bonds that make the polymer more stable to hydrolysis. As the name suggests, these polymers require a temperature cure. The melamine-formaldehyde resin is created by a two step process: the first step is a methylolation which reacts the melamine and the formaldehyde and the second is etherification, a reaction with an alcohol. [21]

The disadvantage to using this system is generally a health and environmental consideration. During cross-linking of the acrylic resin and the MF, formaldehyde gas is produced. If not performed in a location with adequate ventilation, this can cause harm to the user during prolonged exposure. The advantages are the ease of

application, the relatively low curing temperatures, the hard coating formed, and its temperature resistance in application. In underfilm testing, acrylic coatings were found to provide incomplete corrosion protection [22].

2.4 Cobalt

Cobalt was first obtained as an element in 1742 by Brandt [23], although it was used in ancient times as a blue pigment for ceramics and glasses. It is rarely found in pure form in nature, but can be found in trace quantities in many different forms [24]. Thus many source ores are used, which leads to different forms of extraction and refining. In turn this can result in a variety of purity metals which all possess slightly varied properties, behavior, grain size, isotropies, and impurities [24].

Cobalt is an element of the first triad of Group VIII of the periodic table. It possesses an atomic number of 27, an atomic weight of 58.9332 and one stable isotope with a mass number 59 [23]. Its most useful radioiosotope, Co^{60}, is obtained through neutron irradiation of Co^{59}, has a half-life of 5.28 years and emits γ-rays with energies of 1.17 and 1.33 MeV [24].

The anodic reaction of cobalt corrosion leading to dissolution of the metal in aqueous media is

$$Co \leftrightarrow Co^{2+} + 2e^{-}$$

This reaction is usually considered the rate limiting step of the corrosion process in an aqueous environment [25]. The cathodic reaction was stated previously.

Depending on the corrosive environment, different corrosion products will form. These products can be predicted by the Pourbaix diagram for Co which is shown in Figure 2-2 [26]. These diagrams show the theoretical corrosion, passivity, and immunity regions for cobalt, as well as the products formed for a given electrolyte at a given temperature for a set of potential and pH values [26]. Corrosion is favored in the diagram where soluble metal ions are stable. The passivation regime is indicated in the diagram in the region of stable oxides, and immunity results where it is thermodynamically unfavorable for corrosion to occur.

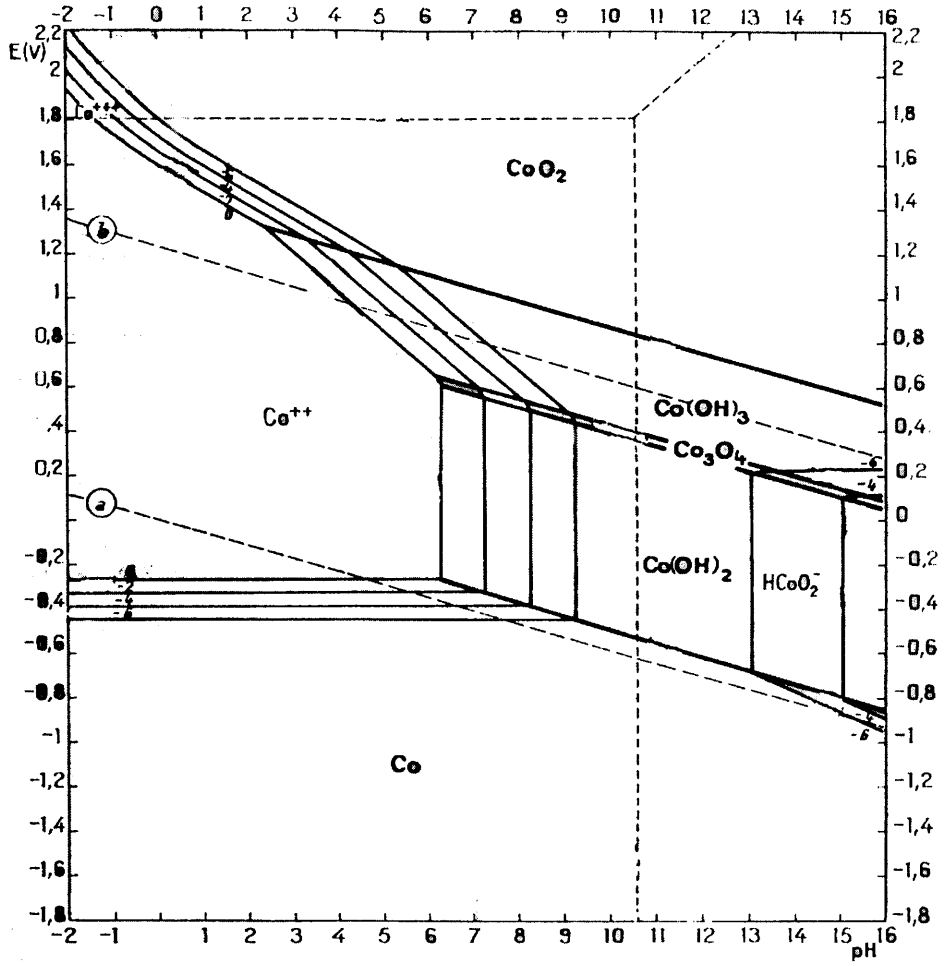

Figure 2-2: Potential-pH Diagram for Cobalt

From Figure 2-2 it can be seen that cobalt is a slightly noble metal. This is evidenced on the diagram by the small common area between the immunity domain of cobalt and the stability domain of water. The stability domain of water occurs between the two dashed diagonal lines, labeled a and b in the plot. These lines correspond to water reactions. The upper line delineates the region where water can anodically form oxygen gas and the lower line indicates where water can cathodically form hydrogen gas. In between the two lines water molecules are stable. [2]

It can also be seen that cobalt is not corrodible in neutral and alkaline solutions without oxidizing agents, is somewhat corrodible in acid solutions without oxidizing agents, and is quite corrodible in acidic or extremely alkaline solutions with oxidizing

agents [26]. In acids such as dilute hydrochloric and sulfuric acids, cobalt will slowly dissolve yielding cobaltous ions and salts; and hydrogen gas [23]. Oxidizing solutions of neutral or somewhat alkaline conditions form an oxide layer, and fuming nitric acid easily passivates cobalt. Unlike the oxides of some other metals, however, a native cobalt oxide is neither very stable, nor protective [27].

These native oxides, which can be formed in air, are usually only about 2 nm thick on the surface of the cobalt. The oxide formed is considered a duplex passive layer, consisting of two different states. The bulk oxide is CoO or $Co(OH)_2$ and the outer layer is CoOOH or Co_2O_3 [28].

2.5 Measurement Techniques

There are a number of different ways to measure corrosion. One of the most basic is a simple mass loss experiment [2] [1]. A specimen is weighed and then exposed to an aggressive environment—an acidic or basic electrolyte, a salt spray, an extremely humid atmosphere. After prolonged exposure, the specimen is weighed again to find the mass loss. From such data, the corrosion rate of a uniformly corroded material can be determined. It is important that corrosion is uniform, because at sites of localized corrosion, such as a pit, the corrosion rate can be extreme compared with the bulk metal; however, due to the small area involved, mass loss would be small.

Not all methods are so simple, and most employed today capitalize on the fact that a corroding system is an electrochemical cell. Most electrochemical experiments employ the three-electrode set-up. The corroding metal is the working electrode, an inert material, typically platinum, is the counter electrode where the complement reaction occurs, and the third electrode, the reference, provides the means for the measurement to be made quantitatively. This reference electrode is necessary because it is impossible to measure an absolute value of a half-cell electrode potential [16]. Thus the potential of the half-cell reaction occurring at the working electrode is measured as a relative potential with respect to the reference. Frequently, the reference electrode is connected to the cell via a solution or salt bridge and a Luggin

probe, with the probe tip very near the working electrode [29]. This is done to reduce the ohmic resistance in the electrolyte which can mask the potential of the cell. A 1 mm distance from probe tip to working electrode surface is considered ideal for most scenarios [2].

2.5.1 Polarization Methods

There are two main types of polarization techniques—galvanostatic and potentiostatic. During a galvanostatic experiment the current is controlled and during a potentiostatic experiment the potential is controlled. The techniques utilized during this project were the potentiostatic and potentiodynamic methods. The central equipment required for this type of experiment is the potentiostat. This adjusts the applied current to control the potential difference between the working and the reference electrodes. Controlled current methods are not generally as useful as controlled potential measurements in producing anodic polarization (E vs. log I) curves in determining active-passive behavior of metals [2].

During a potentiostatic experiment, the potential is held at a specified value while the current is monitored. This type of experiment can also be used to produce a set of incremental potentiostatic measurements to build a polarization curve. Potentiodynamic measurements control the potential change between measurements in a continuous measurement that spans a range of potentials. This yields the same polarization curve as the potentiostatic technique. The general setup for either a potentiostatic or a potentiodynamic scan is presented in Figure 2-3. A is an ammeter, N is a null detector, and P is a potentiometer in the diagram [2].

The polarization curve generated during this type of experiment can be used to determine the corrosion rate. Tafel extrapolation is performed on the curve in the linear region near E_{corr} for both the cathodic and the anodic region. The intersection of the Tafel line at E_{corr} yields the corrosion current, I_{corr}, which is proportional to the corrosion rate. There are limitations to this technique, however. Generally one decade of linearity is required for sufficient determination of the Tafel constant. Also, a steady-state polarization curve is the most useful in assessing the Tafel constants,

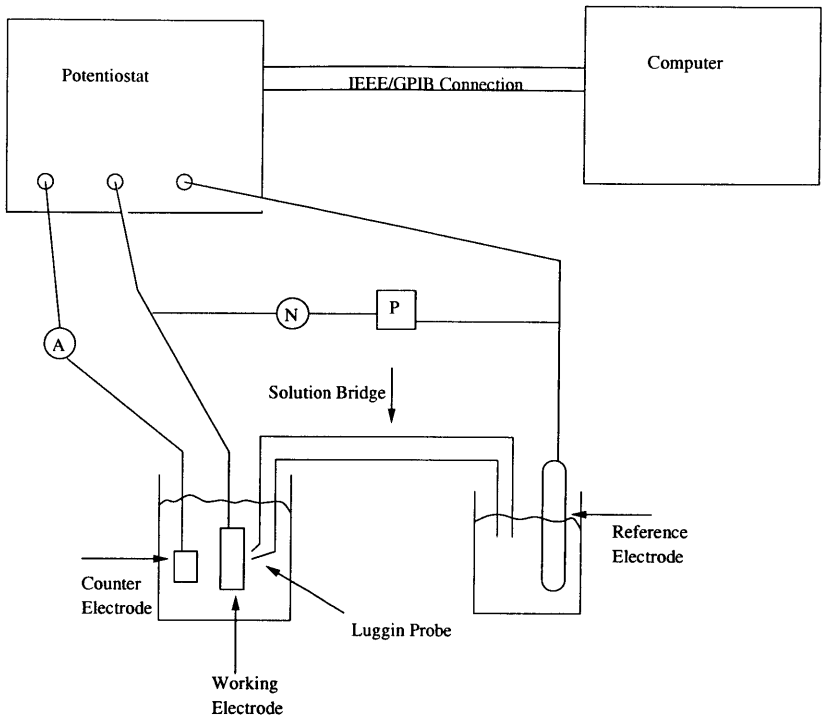

Figure 2-3: Potentiostat Controlled Measurement Setup

but this is not always generated [2]. To try and achieve this, most scans are started after the specimen has been immersed in the solution for some set period of time. Another concern is that irreversible changes to the sample which are due to the measuring process occur, thus affecting later measurements [30].

Linear Polarization

The concept of linear polarization was developed by Milton Stern and his coworkers in the 1950's [16]. Stern and Geary [31] [32] arrived at the following equation:

$$\left.\frac{d\phi}{di}\right)_{\phi \to 0} = \frac{\beta_a \beta_c}{(2.3)(i_{corr})(\beta_a + \beta_c)} \tag{2.2}$$

which equates the slope of a potential-current plot to the Tafel constants and the corrosion current, where ϕ is the potential. A linear relationship was found for potential as a function of current for very small changes in potential with respect to the corrosion potential. The main assumption made here is that both the anodic and

cathodic reactions are charge transfer controlled [16]. Thus the relationship between current and potential is expressed as

$$I = I_{corr}\left\{exp\frac{2.3(\phi - \phi_{corr})}{\beta_a} - exp\frac{-2.3(\phi - \phi_{corr})}{\beta_c}\right\} \tag{2.3}$$

Plotting the same data as a current vs. potential curve yields a similar equation. The slope $\frac{di}{d\phi}$ near E_{corr} is the inverse of R_p, where R_p is the polarization resistance of the corroding metal. Therefore equation 2.2 can be rewritten as [4]:

$$I_{corr} = \frac{\beta_a\beta_c}{2.3(\beta_a + \beta_c)}\frac{1}{R_p} \tag{2.4}$$

Combining equation 2.3 with equation 2.4 yields:

$$2.3R_pI = \frac{\beta_a\beta_c}{\beta_a + \beta_c}\left\{exp\frac{2.3\Delta\phi}{\beta_a} - exp\frac{-2.3\Delta\phi}{\beta_c}\right\} \tag{2.5}$$

with $\Delta\phi = \phi - \phi_{corr}$.

To perform linear polarization, a potentiodynamic scan is conducted in the region of $\pm$ 30 mV from the corrosion potential. The corrosion potential is found by measuring the open circuit potential of the system until the system appears to have reached a steady-state value. The slope of this plot in the region near E_{corr} is then determined to yield a value for R_p. The corrosion current, and thus the corrosion rate, can then be determined once the Tafel constants are known. This can be accomplished in a few steps: 1. plot the left hand side of equation 2.5 vs. $\Delta\phi$, 2. use curve fitting to determine the values of the Tafel constants, and 3. using equation 2.4 calculate I_{corr} [4].

A number of subsequent measurements can be made which lead to information about the corrosion rate, corrosion potential, Tafel slopes, and polarization resistance as a function of time.

2.5.2 Electrochemical Impedance Spectroscopy

The concept of impedance spectroscopy was first introduced in the 1880's by Oliver Heaviside [33]. Impedance spectroscopy characterizes the electrical properties of interfaces and materials through the use of conducting electrodes. Basically, an electrical stimulus is applied to electrodes and the response, which is assumed to be time variant, is observed. An example of a response is the transport of electrons or ionic species. This flow of charged particles in turn depends on the ohmic resistance of the system which is affected by the electrodes, electrolyte, and reaction kinetics at the interface. The most common use of EIS is to measure the impedance in the frequency domain by applying a single frequency voltage to the interface and measuring the phase shift and amplitude of the current at that frequency.

The voltage applied and corresponding current are

$$v(t) = V_m sin(\omega t) \tag{2.6}$$

$$i(t) = I_m sin(\omega t + \Theta) \tag{2.7}$$

where the frequency, $\omega \equiv 2\pi f$, and Θ is the phase difference. Conventional impedance is written as $Z(\omega) \equiv \frac{v(t)}{i(t)}$.

The impedance is most often broken into its real and imaginary forms. A series of useful equations is based on the geometry of Figure 2-4.

$$Re(Z) \equiv Z' = \mid Z \mid cos(\Theta) \tag{2.8}$$

$$Im(Z) \equiv Z'' = \mid Z \mid sin(\Theta) \tag{2.9}$$

$$\Theta = tan^{-1}(\frac{Z''}{Z'}) \tag{2.10}$$

$$\mid Z \mid = [(Z')^2 + (Z'')^2]^{\frac{1}{2}} \tag{2.11}$$

Impedance spectroscopy is only useful when there is a linear response; however, most systems are non-linear. The amplitude of the applied potential difference must be less than the thermal voltage, $V_t = \frac{kT}{e}$. At room temperature a linear response for a bare metal can be approximated with voltage perturbations of $\pm$ 5 mV while

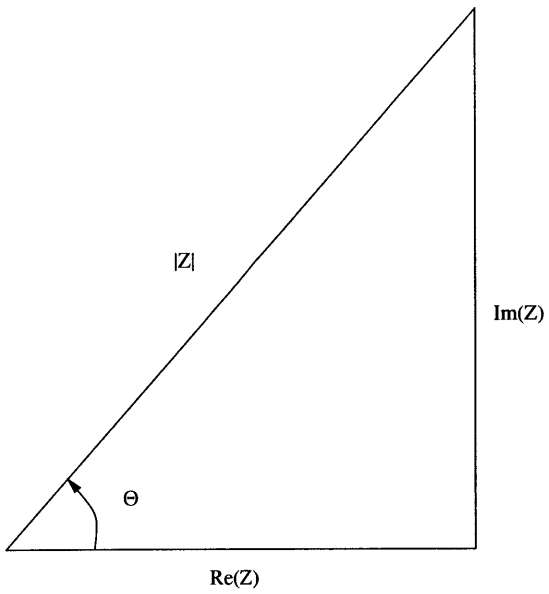

Figure 2-4: Impedance Relationships

for a coated system ± 25 mV is utilized. If the coated system has not undergone too much corrosion it can be considered a linear system and the larger AC signal of ± 25 mV is possible [3]. The larger signal decreases the scatter in the recorded data. Thus this technique is characterized by its small AC fluctuations, which also maintains a measure of a non-destructive testing technique. [33]

The impedance data is relatively simple to generate, and the results can be correlated with many of the complex material variables of the test system. The data is either analyzed with a mathematical model [34] or an empirical equivalent circuit. Conversely, there is a lot of ambiguity in interpretation of the data. For any given set of data, a number of different equivalent circuits may fit, [33] and from these different circuits, different parameter values yield different information about the actual, physical system. Thus, it is important to use an equivalent circuit that closely represents this physical system.

Electrochemical impedance spectroscopy can be used for many different applications, but one of primary interest is its use in the study of the corrosion behavior of coated metals. This is not possible through more traditional electrochemical techniques such as the ones explained previously, due to their poor detection capabilities

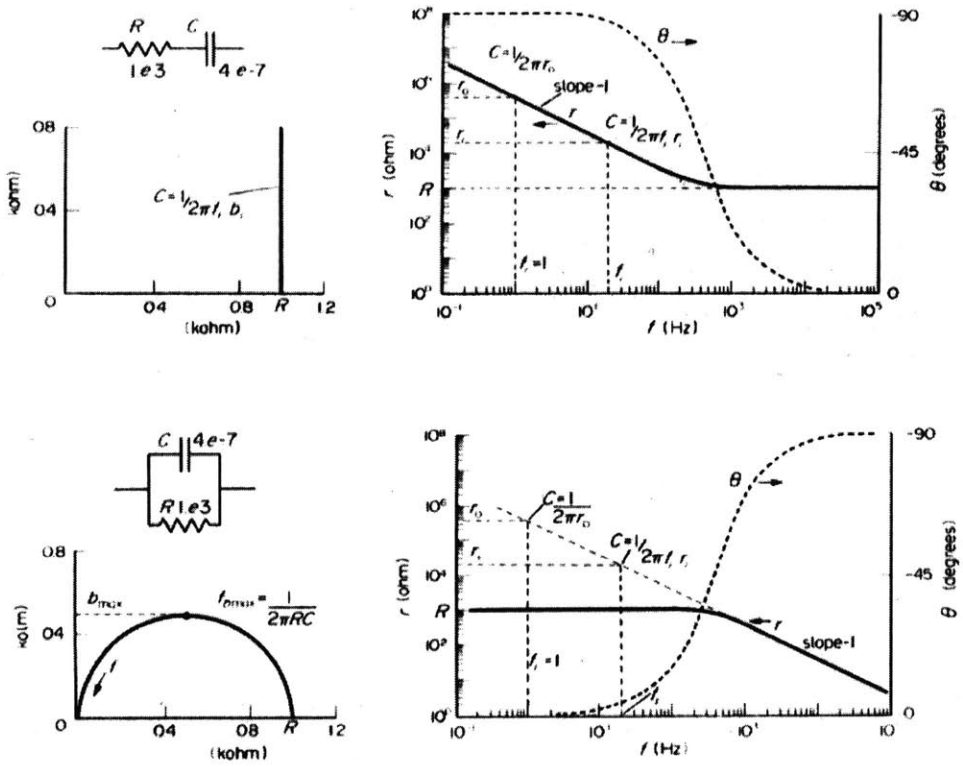

Figure 2-5: RC Circuits and Corresponding Impedance Spectra

in low-conductivity media. In this field of study, EIS is used to rate coatings, look at interfacial reactions, quantify coating breakdown, and predict the lifetime of coating/metal systems [3]. The study of coated systems employs not only the complex plane or Nyquist plot, which is the Z_{im} (the reactive component) vs Z_{re} (the resistive component) [35], but also Bode plots. Bode plots show the impedance modulus and the phase angle as a function of frequency. From these Bode diagrams, the resistances and capacitances of the circuit elements, the experimental system's components and reactions, can be determined. These plots are much more sensitive to changes with frequency than the Nyquist plots [3].

While a real corroding system is never a simple equivalent circuit, the best way to describe the interpretation method of equivalent circuits is to start simplistically. A parallel RC circuit and a series RC circuit are the most basic. The circuits and their corresponding plots are shown in Figure 2-5 [35]. The complex plane plot of a series

RC circuit is a vertical line. The corresponding Bode plot of modulus is a horizontal line in the high frequency range switching to a linear curve with a slope of -1 at lower frequencies. The horizontal portion represents the resistor while the slope of -1 is a pure capacitor. The parallel RC circuit has a complex plane plot of a semicircle with a diameter of the resistance. The Bode modulus plot is the reverse of that for the series circuit. The phase plot is close to 90^o when the capacitive element is exhibited and an angle close to 0^o when the behavior is resistive. [35]

The more complex behavior of a corroding coated system is built upon these basic circuits. A coated system must take into account the solution resistance, R_Ω, pore resistance in the coating, R_{po}, the capacitance of the film, C_c, the double layer capacitance at the interface, C_{dl}, and the resistance of the charge transfer at the interface, R_{ct}, sometimes taken as the polarization resistance. These last two are attributed to the metal. Another complicating factor that must be accounted for is the possibility of diffusion within the system. This is usually represented by a Warburg impedance. In the complex plane plot this is commonly manifested as a tail at the low frequency end of the semicircle which exhibits a 45^o angle [35] for a sample with a planar surface.

An example of the spectra for a coated sample and equivalent circuit can be seen in Figure 2-6 [3]. The equivalent circuit shown here has the following elements: R_Ω which is the solution resistance, R_{po} the pore resistance, R_p the polarization resistance, C_c the coating capacitance, and Cdl the double layer capacitance at the metal/coating interface where corrosion occurs. The capacitance of the polymer is defined by

$$C_c = \frac{\epsilon \epsilon_o A}{d} \tag{2.12}$$

where ϵ is the dielectric constant of the polymer and ϵ_o is the dielectric constant of free space, A is the exposed area of the working electrode, and d is the thickness of the coating. Most impedance models for coated systems are similar to this equivalent circuit, perhaps with more complicated elements embedded in the circuit such as a Warburg impedance. The corresponding Bode plot in Figure 2-6 presents the modu-

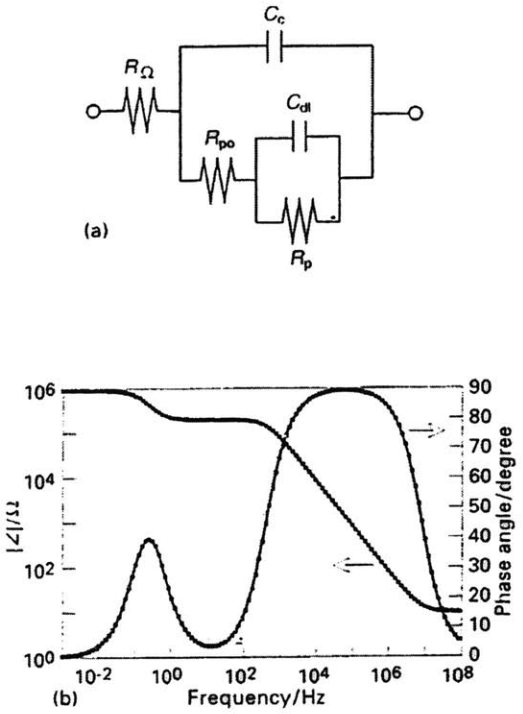

Figure 2-6: Equivalent Circuit and Corresponding Bode Plots for Coated System

lus of the impedance and the phase angle over the measured frequency range. From this plot the values for the circuit are determined. In the modulus representation the plateaus represent resistance and the linear portions with a slope of -1 represent capacitances. The component termed R_p is actually R_{ct}, the charge transfer resistance, but it can be related to the polarization resistance, and thus the corrosion rate. The coated system shown here has two time constants, $\tau \equiv RC$, represented as peaks in the phase spectra. The time constant at the high frequency contains information about the polymer coating and the time constant at the low frequency contains information about the metallic substrate. The high frequency resistive plateau is R_Ω, the mid-frequency one corresponds to $R_\Omega + R_{po}$, and the low frequency plateau is $R_\Omega + R_{po} + R_p$. Taking the difference of the latter two yields the R_p value which can be related to the corrosion curent and the mass lost by the system. The first capacitive portion of the modulus plot gives information on C_c, while the second does the same for C_{dl}.

When studying a coated system, the impedance spectra changes with time. Initially an intact coating can be detected. Subsequently, water and ionic species diffuse through the polymer. This will lead, ultimately, to corrosion initiation. Once the corrosion of the metal begins, the EI spectra can exhibit significant variations. This is dependent on the type of corrosion that occurs and whether it is accompanied by delamination or not. From the data, corrosion rates can be estimated, using determination of R_p and the charge transfer resistance. The determination of rates is not, however, as simple as those performed with DC techniques, and care must be taken to understand the corroding system during interpretation of the data [30]. The main benefit of EIS relative to DC tests is that EIS measurements have a frequency component which can provide mechanistic information [2].

2.6 Experimental Setup

The electrochemical measurements performed in this study were of two types: DC and AC. The DC tests performed were potentiodynamic and potentiostatic scans and linear polarization. The AC tests performed were electrochemical impedance spectroscopy.

2.6.1 Samples

There were two main types of samples studied: coated metal and non-coated metal. Within each sample type there were two categories, foils and wafers. The metal of choice was cobalt. Cobalt was chosen because of its magnetic properties. The foils used were 0.25 mm thick, 99.95% pure in an as-rolled condition from Alpha Æsar. The wafer samples were 10 cm diameter silicon wafers with an e-beam deposited layer of 99.95% pure cobalt from a target produced by Pure Tech, Inc. The wafer samples were made by the Microsystems Technology Laboratory (MTL) at MIT. The depth of the cobalt coating on the wafers was measured by profilometry on a Tencor-KLA P10. First kapton tape was placed on a monitor silicon wafer before cobalt deposition. After the cobalt was deposited, the tape was removed and the depth difference was

measured. The thickness was determined to be 3200 $\AA$. This thickness, while thicker than that used in most microelectronics, was chosen to avoid problems with sheet resistance, which is known to cause ohmic error during electrochemical testing [28].

A polymer coating was then applied to some of the samples. The foil and wafer samples were coated with a transparent acrylic varnish. The varnish was mixed from Viacryl VSC 5754/60 and Maprenal MF800 both from Vianova Resins. Viacryl is an acrylic emulsion of 60% acrylic in butylacetate. Maprenal is a melamine-formaldehyde of 72% MF in iso-butanol. The mix ratio was 36 g MF to 100 g of resin. Acetone was added to the mixture to produce the right amount of fluidity before application. Greater amounts of acetone were utilized to make the varnish more fluid during application, decreasing the thickness of the polymer. The samples were then dipped into a bath of the varnish and allowed to air dry for a short time prior to curing in an oven at 150 ^{o}C for 30 minutes. The curing time was systematically altered to provide a different defect density in the coatings. Thus, the time to coating failure could be decreased and the corrosion initiation rate increased. By lowering the cure time, the number of cross-links formed decreased, making the polymer more permeable to moisture and ions. Thus the undercured polymer was more readily attacked by the test solutions. The thickness of the coating on the foils was measured with a magnetic induction coating thickness measurement system. The range of thicknesses was 15-30 μm. The wafer samples were unable to be measured in this fashion due to their composite nature. They were coated at the same time and in the same manner as the foils and the thickness was assumed to be the same.

A number of wafer samples were coated with a polyimide coating. This process was also performed by MTL. The polyimide used was Pyralin PI 2556 from DuPont. The coating process consisted of a spin-coating process followed by a soft bake and then a cure cycle. This cure is the imidization reaction and should be performed in a controlled environment oven free from oxygen which could cause oxidation of the metal substrate at high temperatures. The temperature of the acrylic varnish was sufficiently low to avoid this problem. The polyimide can be fully cured at 180 ^{o}C, but higher temperatures are used to achieve the best electrical and mechanical properties

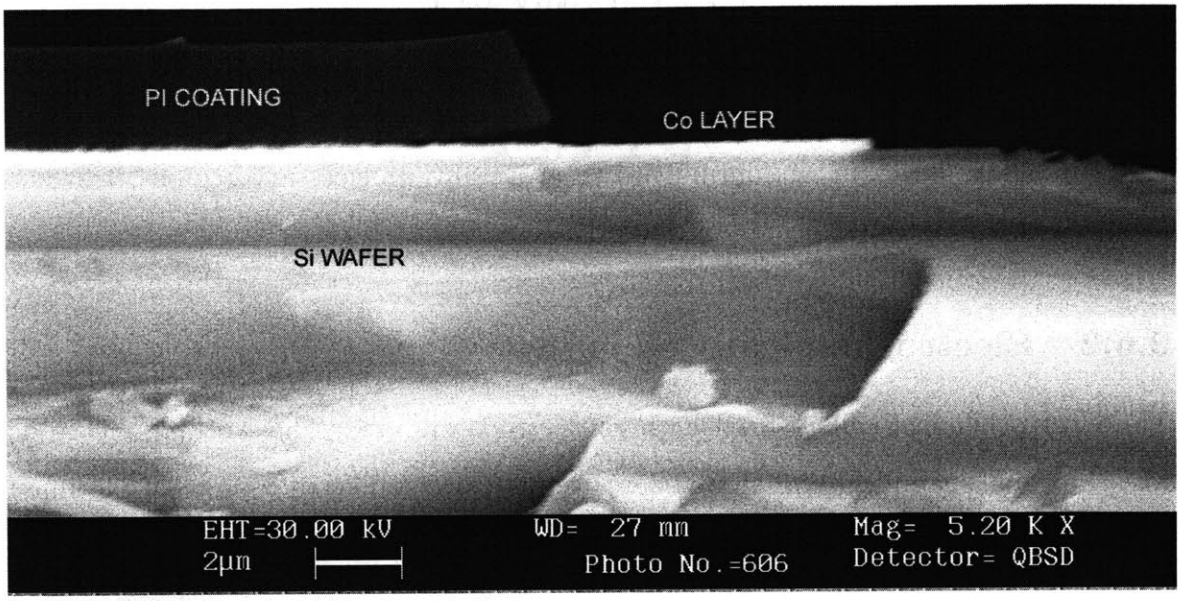

Figure 2-7: SEM Cross Section of PI-Coated Cobalt-Silicon Wafer

of the polymer. A cross section of a polyimide coated wafer sample is shown in Figure 2-7. Three distinct layers are visible; the dark upper layer is the PI coating, the thin bright layer in the middle is the cobalt, and the large lower layer is the silicon wafer. This image was taken of a sample that was fragmented in liquid nitrogen and then viewed by SEM.

The samples, bare or coated, were sectioned into pieces approximately 1.5 cm by 1.2 cm. The foils were cut with scissors while the wafers were cut with a scribe and snap technique. The silicon side of the wafer sample was marked using a carbide scribe. A small amount of force was then applied to the sample to snap the piece at the scribe mark.

For electrochemical testing the samples needed to have a wire attached for connection with the equipment. A thin copper wire with an insulating sheath was used. At the attachment point the wire was stripped and then adhered to the metal surface using either silver epoxy or silver paint. The silver epoxy provided a better mechanical bond while the silver paint allowed for a quicker dry time. For the coated samples a region of the polymer was removed prior to wire attachment. For samples using

silver paint, a small amount of 5-minute epoxy was then applied to the attachment region for more stability. And finally a grey paint, Ameron's Amercoat 90, which is a mixture of a resin and cure in a 4:1 volume ratio, was applied to the wire attachment area as well as edges or discontinuities to avoid any unnecessary regions in which localized corrosion could occur.

2.6.2 Electrochemical Cell

The electrochemical cell utilized a three-electrode system. The working electrode was the cobalt sample. The auxiliary or counter electrode was a piece of platinum foil, and the reference was a saturated calomel electrode (SCE). This electrode is a solution of mercurous chloride, Hg_2Cl_2, and liquid mercury in contact with a saturated potassium chloride, KCl, solution. A platinum wire in the mercury allows for an electrical contact. The corresponding half-cell reaction with this electrode is

$$Hg_2Cl_2 + 2e^- \leftrightarrow 2Hg + 2Cl^-$$

All potentials reported here were measured with respect to this electrode. This electrode has a potential of +0.241 V vs. SHE. SHE is a standard hydrogen electrode which has a potential defined as 0.00 V for the reaction

$$2H^+ + 2e^- \leftrightarrow H_2$$

For the potentiodynamic and potentiostatic experiments, the reference electrode was in a separate vessel from the working electrode. The connection was made with a solution bridge and a Luggin probe, similar to the setup in Figure 2-3. For the EIS experiments, the counter electrode was wrapped around the working electrode and they were placed directly into the solution that was in contact with the working electrode, as demonstrated by Figure 2-8. The vessel used for the EIS experiments was a 60 ml syringe with the tip cut off. This provided an area small enough for the sample size, and a volume large enough to contain the electrolyte solution and the

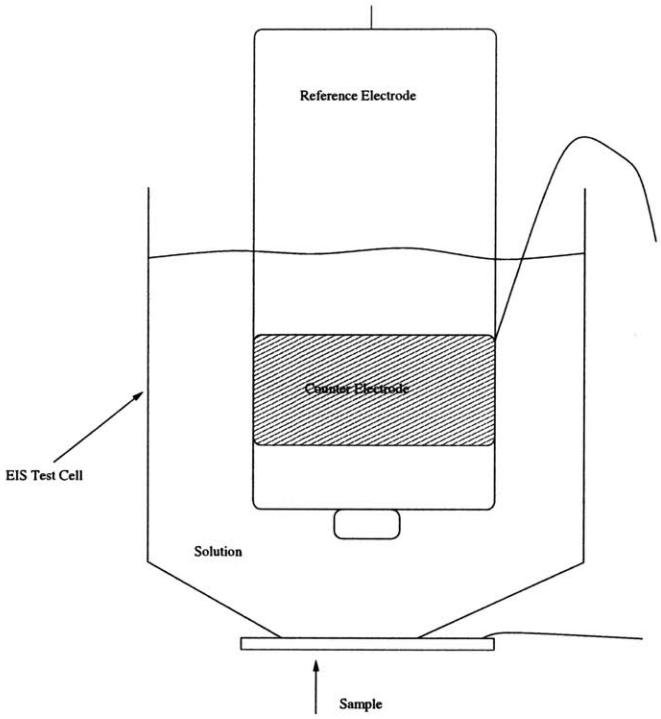

Figure 2-8: EIS Test Cell

other two electrodes.

Two test solutions were used—0.5 M NaCl and acidified NaCl. The solutions were made up from reagent grade NaCl and DI water in volumetric flasks. The second solution was made with HCl and the base NaCl solution. The solution was adjusted to a pH in the range of 2–3.

2.6.3 Equipment

Potentiostatic and Potentiodynamic Scans

For the potentiodynamic and potentiostatic scans, as well as the linear polarization tests, the potentiostat used was a Schlumberger Solartron 1286 Electrochemical Interface. The potentiostat was joined to a PC by an IEEE/GPIB connection. The scans were performed using the electrochemical software, DC Corrware from Scribner Associates. The majority of the analysis was carried out using this same software or in Microsoft Excel.

Electrochemical Impedance Spectroscopy

The EIS tests were carried out with a Schlumberger Solartron 1287 Electrochemical Interface and a Solartron 1260 Impedance/Gain-Phase Analyzer joined to a computer through an IEEE/GPIB connection. The software used to perform tests was ZPlot and the corresponding analysis package ZView, both from Scribner Associates.

2.7 Results and Discussion

2.7.1 Potentiodynamic and Potentiostatic Scans

The polarization curves for the cobalt samples were performed either in 0.5 M NaCl or in the same solution acidified with HCl to a pH in the range of 2-3. Potentiodynamic curves were generated at a scan rate of 1 mV/s. Before beginning the scan, the open circuit potential of the solution was monitored for at least 10 minutes after sample immersion. Scans were initiated in the cathodic region about -250 mV relative to the corrosion potential and continued into the anodic region to a potential of 700 mV with respect to the reference electrode. Representative curves for both a foil sample and a wafer sample in 0.5 M NaCl are shown in Figure 2-9. Figure 2-10 presents polarization curves for foil samples in the two different electrolytes. Table 2.1 lists the corrosion potential, E_{corr}, the corrosion current, I_{corr}, and the anodic and cathodic Tafel constants, β_a amd β_c for the three different sample types: wafer in 0.5 M NaCl, foil in acidified NaCl, and foil in 0.5 M NaCl.

Sample	E_{corr}	I_{corr}	β_a	β_c
wafer in 0.5 M NaCl	-350 mV	1.8 e^{-5} A	60 mV/decade	180 mV/decade
foil in acidified solution	-260 mV	4.1 e^{-6} A	40 mV/decade	170 mV/decade
foil in 0.5 M NaCl	-370 mV	1.7e^{-6} A	70 mV/decade	160 mV/decade

Table 2.1: Electrochemical Data

The potentiodynamic curves for the foil and wafer samples are presented in both Figure 2-9 and Figure 2-10 An example of corroded surface can be seen in Figure 2-12.

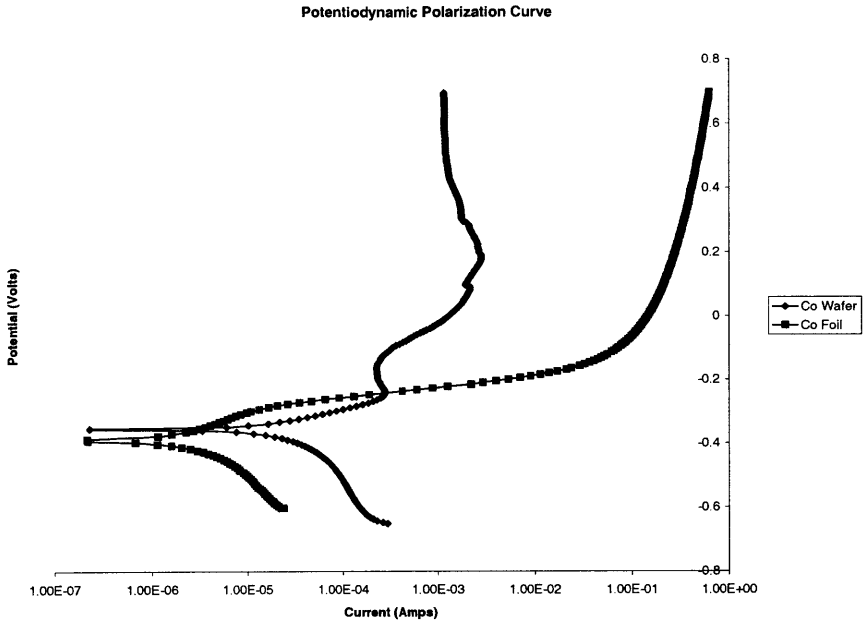

Figure 2-9: Polarization Curves in 0.5 M NaCl for Foil and Wafer Cobalt Samples

The curve for the silicon wafer with deposited cobalt, exhibits a decrease in current in the potential range -240 to -100 mV, which is a tendency towards passivation. This was also noticed in some nickel-cobalt alloy thin films and bulk samples by other researchers [6]. The passive film that is likely formed here is quickly dissolved as the curve returns to an active state. At higher potentials, the current for the wafer sample decreases again, above 190 mV. This is likely due to the removal of most of the cobalt layer, revealing the silicon substrate. Upon completion of such a potentiodynamic scan, the mass loss for the wafer samples was in the range of 60% and the silicon substrate was visible in some regions. Some wafer samples were prepared with cobalt deposited to a thickness of 300 Å. When potentiodynamic scans were performed on them the scan removed nearly all of the cobalt, to an even greater degree than the 3200 Åsamples. It was determined that these samples would not be the most suitable for use in this project.

The corrosion potential determined from Figure 2-9, and others generated for foils

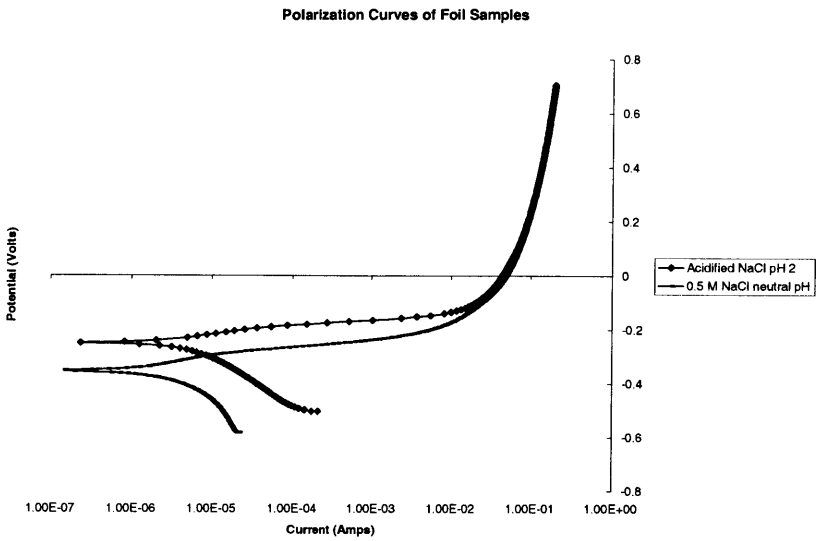

Figure 2-10: Polarization Curves for Cobalt Foil Samples in Both Solutions

are in the region of -360 mV to -380 mV vs. SCE. From these plots, Tafel slopes were also calculated. These are 70 ±15 mV/decade for the anodic region and 160 ±15 mV/decade for the cathodic region. These values are in reasonably good agreement with values reported in the literature [36]. It should be noted that there is a slight difference in the corrosion potential between the cobalt wafers and the cobalt foils. There is a more considerable difference in the current, both the corrosion current and the current corresponding to voltages greater than -200 mV. These differences are due to the thickness of the material as well as the structure. The wafer samples have a deposited cobalt layer which has some oxide content, as well as a smaller grain size [36]. This grain size can cause more homogeneous properties in the material. The corrosion potential for cobalt on silicon wafers is about -350 mV vs. SCE while the Tafel slopes are 60 ±10 mV/decade in the anodic and 180 ±10 mV/decade in the cathodic regions. It should be noted that the numbers reported here and the plots are in current, not current density. While the dimensions of all the samples used in these

potentiodynamic tests were the same, the surface area of the wafer and foil samples are different. This is due to the surface roughness of the foil samples.

It can also be seen in Figure 2-10 that there is a change in the corrosion potential and corrosion current with a change in the electrolyte solution. This is due to the pH difference of the electrolytes, as well as the difference in concentration of chloride ions which affect the equilibrium of the anodic and cathodic reactions. In the acidified solution E_{corr} is -260 mV vs. SCE and the Tafel constants are 40 mV/decade and 170 mV/decade for the anodic and cathodic regions, respectively. The corrosion rate in the acidified solution is greater than in the neutral NaCl solution, and the corrosion potential is more negative.

Some cobalt wafer samples were tested in the 0.5 M NaCl solution yielding good results, while others did not. In the acidified solution, however, all the wafer samples behaved in an unusual manner. About 3 minutes after immersion, during an open circuit potential test the cobalt started to peel and flake off of the wafer. Some of the wafer samples showed similar behavior in the 0.5 M NaCl solution, even in DI water. This could be an artifact of the cobalt deposition process, or the bond between the cobalt and the silicon could have been aggressively attacked by the acidic solution. The most probable scenario is that the cobalt is poorly adhered to the wafer and the deposited cobalt layer is under stress such that the moisture upsets the precarious system, causing the cobalt layer to delaminate. All subsequent tests were performed solely in the 0.5 M NaCl solution, with the batch of wafers that exhibited no delamination when exposed to this environment.

Potentiostatic scans were carried out on both types of samples. These scans were performed at a specific potential and recorded the current with time. An example of a potentiostatic scan of a foil is presented in Figure 2-11. This reveals the change in current with time, and was performed at -170 mV vs. SCE, in the anodic region with respect to E_{corr}. The curve appears to plateau at a reasonably level current after a short period of time. This would indicate that the corrosion rate for this scan is quite constant.

These scans were used to determine the mass loss of the sample. Integrating to

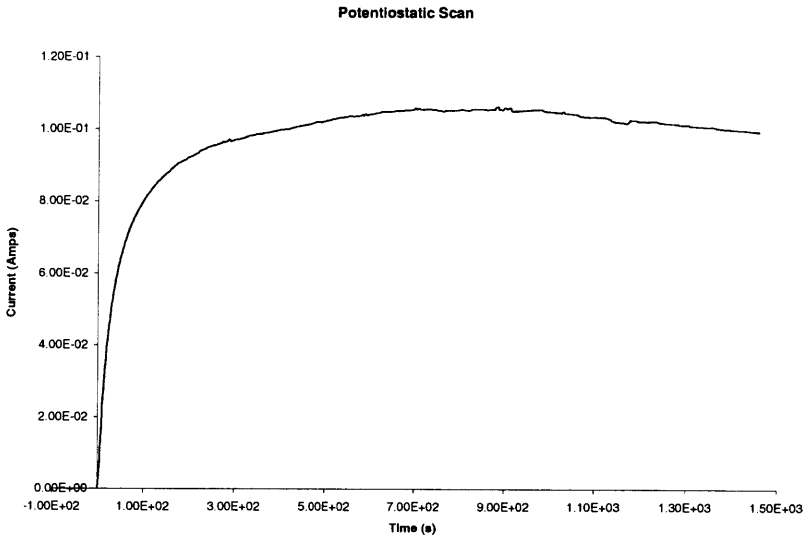

Figure 2-11: Potentiostatic Scan Performed at -170 mV vs. SCE

find the area under the curve yields the number of coulombs lost by the sample. In this particular sample 142.9 coulombs were lost. Using the following equation

$$m = \frac{Ita}{nF} \tag{2.13}$$

yields m, the change in mass, where I is the current, t is time, a is the atomic mass, n is the valence change of the metal in the reaction, and F is Faraday's constant, 96,500 C/equivalent. For cobalt the atomic mass, a, is 58.93 g/mol and the valence change is 2. Thus 0.0436 g of mass were lost by the sample from Figure 2-11.

In some instances, a specific mass loss was desired. Then equation 2.13 was utilized to determine the number of coulombs that needed to be lost by the sample. From that information, the potential and time necessary to run the potentiostatic scan could be approximated from a previously generated polarization curve, such as Figure 2-9.

Figure 2-12 shows a cobalt foil sample that was corroded during a potentiodynamic scan in acidified NaCl; it is representative of most of the samples corroded in this

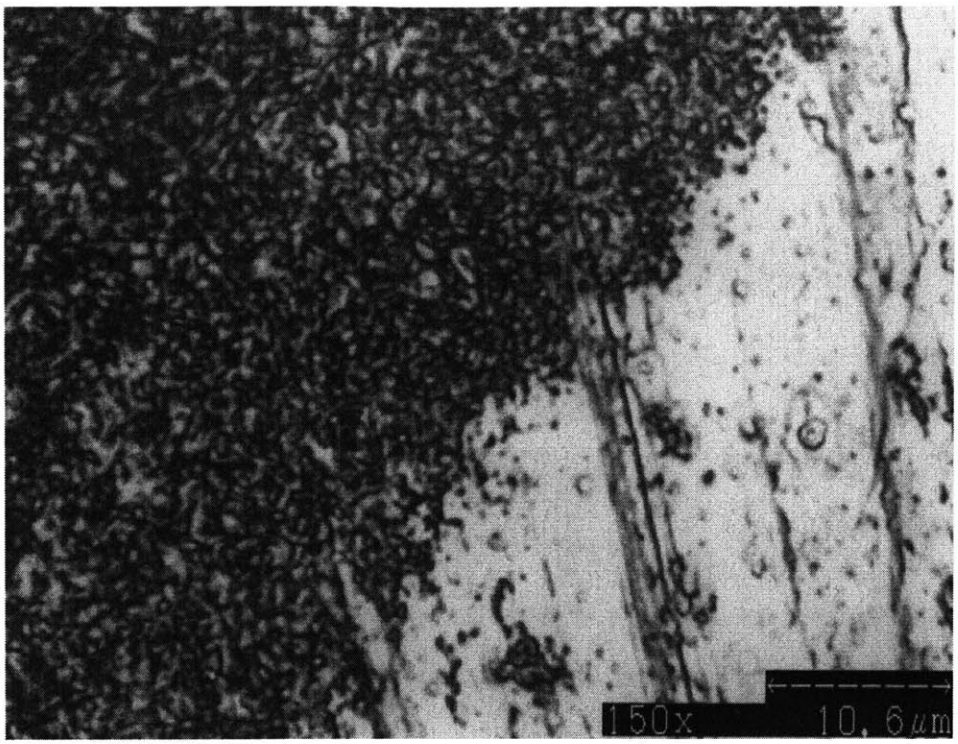

Figure 2-12: Uniform Corrosion in Acidified Solution

solution with this technique. The surface of the metal contains many lines from the rolling performed during processesing of the foil. No polishing was performed before testing the samples, they were maintained in the as-received state. The sample shows a good deal of uniform corrosion on the surface. The image was taken on a Lasertec confocal laser scanning microscope, 1LM21 series, at a lens magnification of 150x. The lighter, right-hand side of the image is an uncorroded part of the surface, and is quite reflective while the darker, left-hand side is the corroded region. Figure 2-13 shows a cobalt foil sample that was corroded in 0.5 M NaCl during a potentiostatic scan. The surface exhibits the same roughness seen in Figure 2-12, but the corrosion is due to pitting, a common localized corrosion mechanism in halides. It appears that the corroded region in Figure 2-13 is due to the coalescence of pits. This image was taken in the confocal laser scanning microscope with a lens magnification of 80x.

The samples used were also weighed before and after the electrochemical experimentation. This was performed on a Mettler AE 200 balance. The gravimetric mass

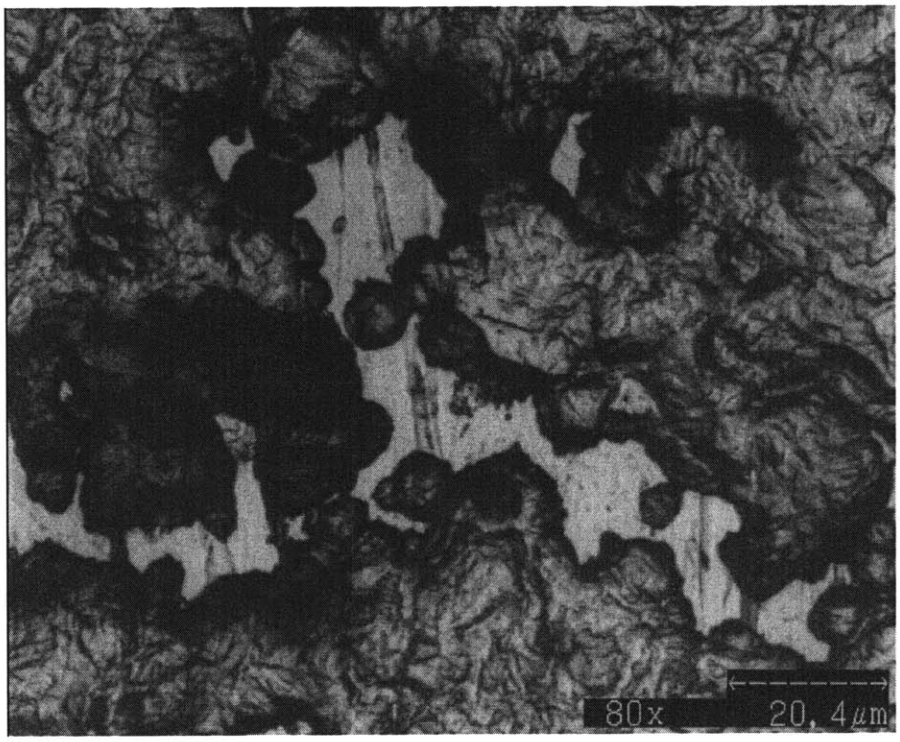

Figure 2-13: Pitting Corrosion in 0.5 M NaCl

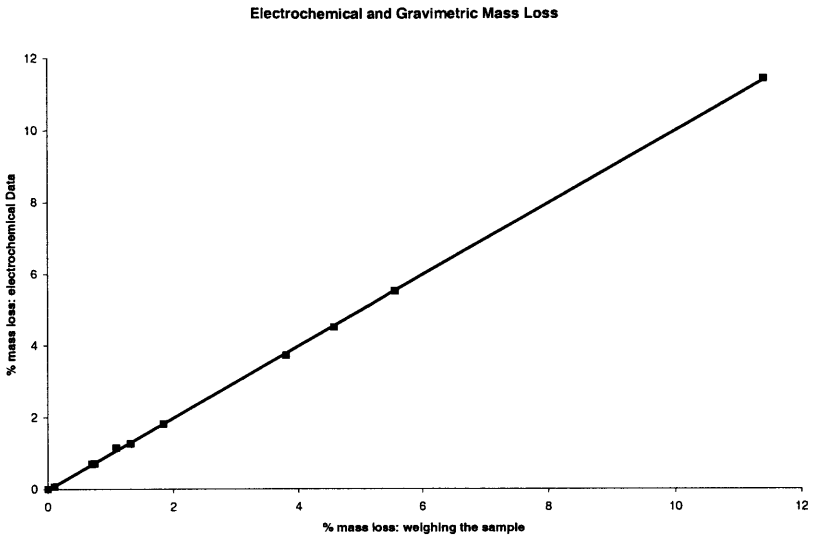

Figure 2-14: Comparison of Electrochemical and Gravimetric Mass Loss Data

loss data was compared with the mass loss calculated from the electrochemical data. This is presented in Figure 2-14. The comparison between the gravimetric and electrochemical mass loss is excellent. When plotted against each other, the two yield a linear curve with a slope of one. The equation for the trend line shown in Figure 2-14 is $y = 0.9974x$ with an R^2 value of 0.9998. It should be noted that the mass loss in question reflects only the loss of cobalt, irrespective of the cobalt corrosion product, or the type of corrosion occuring. The samples were immediately rinsed with distilled water to remove any lightly adhering products or any remaining salt solution. If the rinse did not appear to be clean then the samples were subjected to an ultrasonic clean to remove any significant amounts of oxide or hydroxide left on the surface.

Another interesting aspect to this electrochemistry is the product that is formed during the corrosion. The product arising from corrosion in the 0.5 M solution generally gives the solution a bluish tint, initially. With time, sediment of a greenish-blue color precipitates out of solution. Within a day this precipitate changes to green and

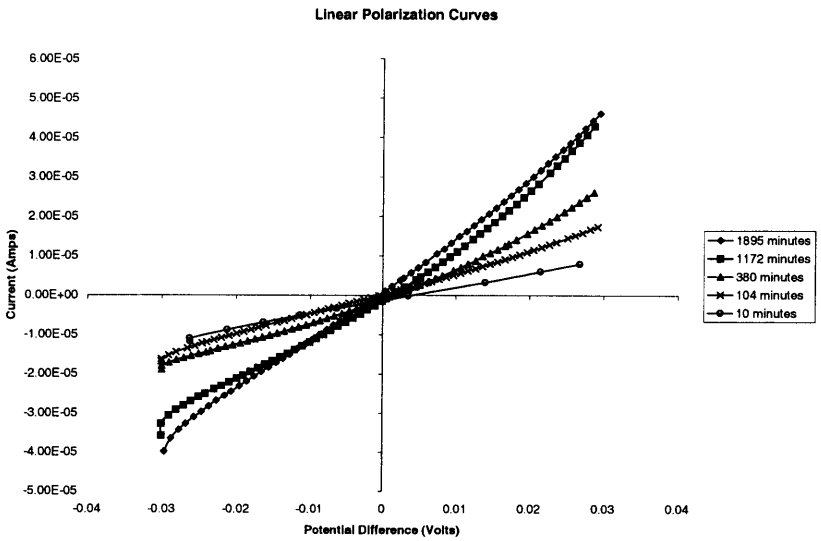

Figure 2-15: Linear Polarization Curves Generated at Different Times

then after a week becomes a greenish-yellow. After months the sediment is a brown color. In the acidified solution, the product gives the solution a pinkish tint, with no sediment precipitating. The difference is due to the pH of the solution. Consulting the Pourbaix diagram [26], Figure 2-2, it can be noted that the acidified solution is in a region of corrosion that yields a product of Co^{++}, the coblatous ions, which remain in solution. The neutral solution of 0.5 M NaCl has a product of $Co(OH)_2$. The colors observed also match colors cited in the literature [26] [23]—cobaltous ions are pink, dicobaltite ion ($HCoO_2^-$) is blue, and the subsequent oxide, CoO, varies between green, brown, grey, and black. The hydroxide formed in a sodium chloride solution is often a blue precipitate which can be oxidized by atmospheric oxygen to $Co(OH)_3$ which is brown in color [23]. The aforementioned hydroxide precipitates in neutral pH, around 6.8.

2.7.2 Linear Polarization

Linear polarization curves were performed on bare cobalt foil samples in the acidified sodium chloride solution. The acidified solution was chosen because cobalt has a greater corrosion rate in this solution than in the neutral sodium chloride. Upon immersion of the sample, the open circuit potential was monitored and after ten minutes the first polarization curve was generated. Each linear polarization resistance scan was performed spanning the region $\pm$ 30 mV from the measured open circuit potential. The scan rate was 2 mV/s. Measurements were made at intervals and, in total, the experiments lasted approximately 30 hours. Figure 2-15 shows several of the polarization curves obtained during an experiment, note the x-axis is the potential difference with respect to the corrosion potential. The slope of these curves yielded the inverse of the R_p values. The slopes increased with time, thus the R_p values were decreasing with time. It should also be noted that the open circuit potential changed with time since the system was dynamic, so the potentials the linear polarization runs were performed at were slightly different for each run. This did not affect any results since everything was calculated with respect to the potential difference.

The left hand side of equation 2.5, $2.3R_pI$, was plotted against the change in potential, $\Delta\phi$. From this experimental curve, computational curve fitting was carried out to determine the values of the Tafel constants. This was performed in Microsoft Excel using the Solver application. Initial estimates of the Tafel constants were chosen based on values from the potentiodynamic scans previously generated. These values were then used to calculate the right hand side of equation 2.5 for the corresponding sets of I and ϕ generated during a polarization scan. The summation of the squares of the differences between the two sets of data, the computed right and left hand sides of equation 2.5, was calculated. This was then minimized, while varying the Tafel constants β_a and β_c for numerous iterations. The computer thus found the best values for the Tafel constants based on the experimental data, while minimizing the error between the theoretical or calculated curve and the experimental curve. An example of both of these curves plotted together can be seen in Figure 2-16.

Once values of the Tafel constants and the polarization resistance were known, the corrosion current for each polarization measurement within an experiment was

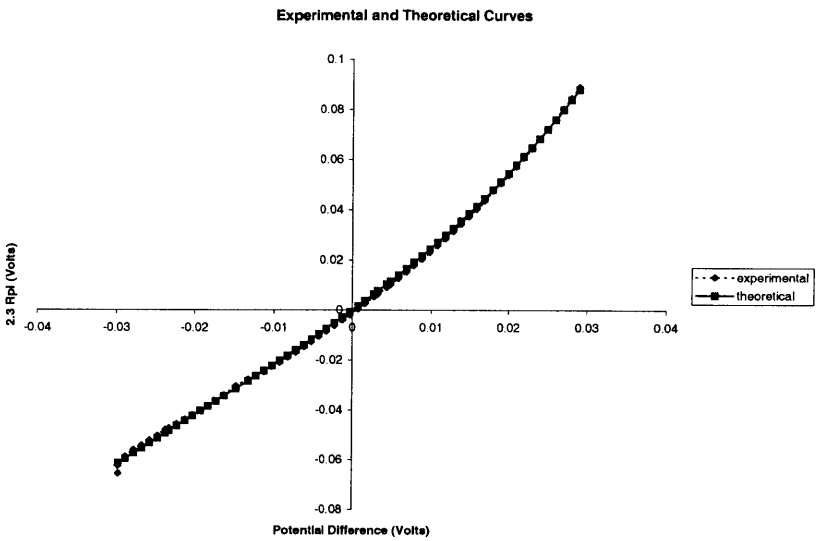

Figure 2-16: Comparison Between Experimental and Theoretical Plots

determined from equation 2.4. This information shows the change in the corrosion current, and thus the corrosion rate, with time. The corrosion current with time is plotted in Figure 2-17. The current trend reveals a steady increase with time. The current also tracks the behavior of the inverse of R_p, determined as the slope of the curves in Figure 2-15. This behavior, $I_{corr}\alpha\frac{1}{R_p}$, is regularly observed for metals, as shown by the literature [4] [37]. Once I_{corr} is known, the actual rate can be determined from the equation

$$r = \frac{m}{tA} = \frac{ia}{nF} \tag{2.14}$$

which is merely equation 2.13 divided through by t and A. A is the surface area of the working electrode, i is the current density, and r is the rate. The area under the curve in Figure 2-17 can be determined to find the mass loss, just as in other I vs. t plots.

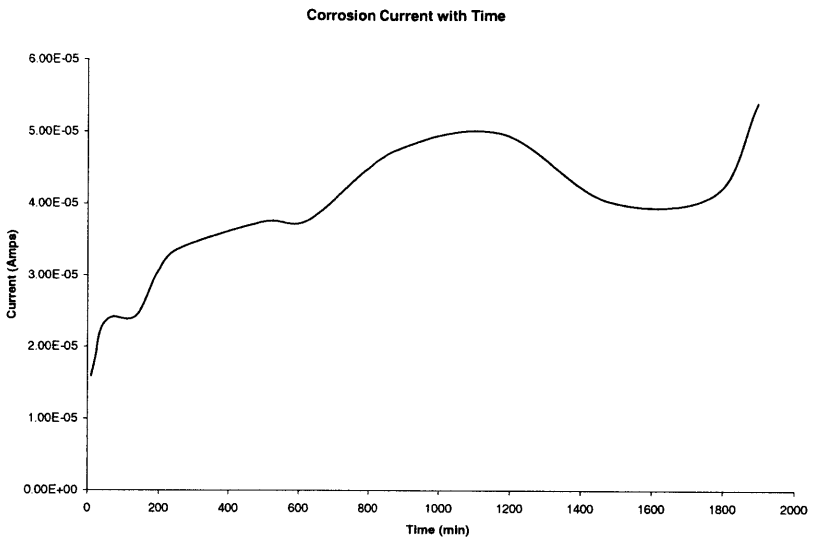

Figure 2-17: Corrosion Current With Time

2.7.3 Electrochemical Impedance Spectroscopy

Electrochemical impedance spectroscopy sweeps were performed on samples in the frequency range from 50 kHz to 20 mHz. The AC voltage perturbation was ± 25 mV for coated samples and ± 5 mV for bare samples. These values were small so as to maintain the assumption of linearity for the system.

Before coated samples were tested, bare cobalt foils were examined in 3.5% NaCl, to see the behavior of the cobalt. The results can be seen in Figure 2-18. The complex plane plot shows a semicircle that on the whole increases in diameter with time, although individual mesurements show a fluctuating diameter. Measurements were made initially, after 45 minutes, 90 minutes, 16 hours, 21 hours, and 40 hours. The modulus plot indicates a resistive plateau around 10^4, this is approximately the R_p value for this sample. The mass loss resulting from this corrosion was quite small, and not detectable on the balance. The complex plane plot also shows a linear extension of the semicircle in the low frequency region, this extension, or tail, is

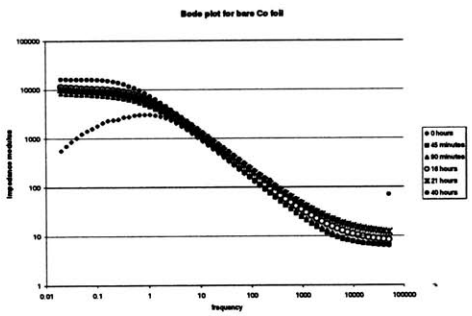

(Bode Modulus)

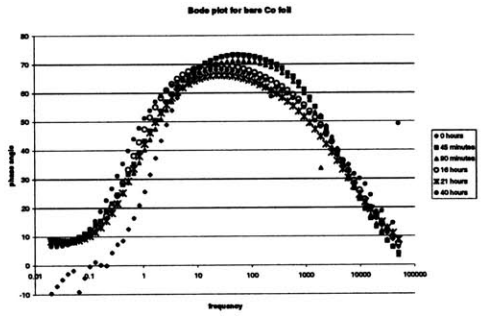

(Bode Phase)

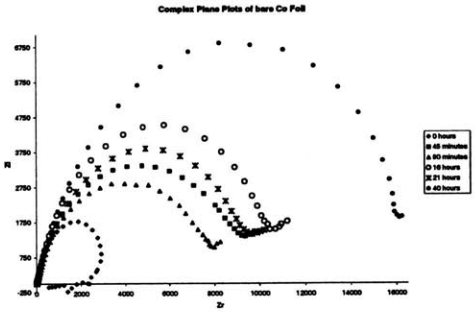

(Complex Plane)

Figure 2-18: Bare Cobalt Foil Impedance Spectra

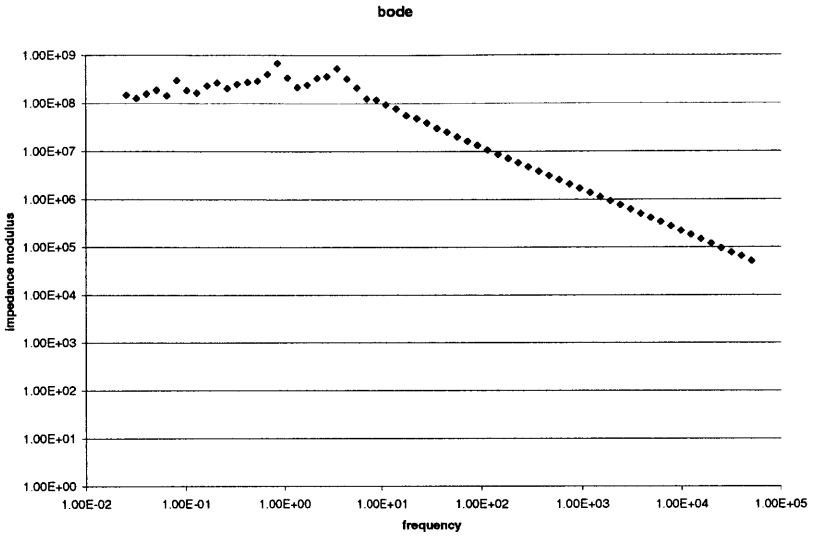

Figure 2-19: Initial High Impedance of the Acrylic Coating

the manifestation of a Warburg impedance. The Warburg impedance indicates the presence of diffusional processes at the metal surface.

Initial tests were performed on coated foil samples in 3.5% NaCl to determine the effectiveness of the acrylic coating. The first samples took a few days before the appearance of anything but capacitive behavior on the Bode modulus diagram. This is shown in Figure 2-19. The low frequency part of the spectra has an impedance above the measurement limit of the instrumentation. This is seen in the scatter of the spectra above 10^8. The impedance of the coating was so high that determining the open circuit potential of the system was difficult, and definitely not influenced by the E_{corr} of the metal. The potential for the experiment was set at the open circuit potential for cobalt, determined by polarization methods, until the open circuit potential of the system could be measured. Finally the second time constant, indicative of the embedded circuit of the the metal, appeared. The corrosion initiated in the processing scratches on the surface of the foil. This can be seen in Figure 2-20 which

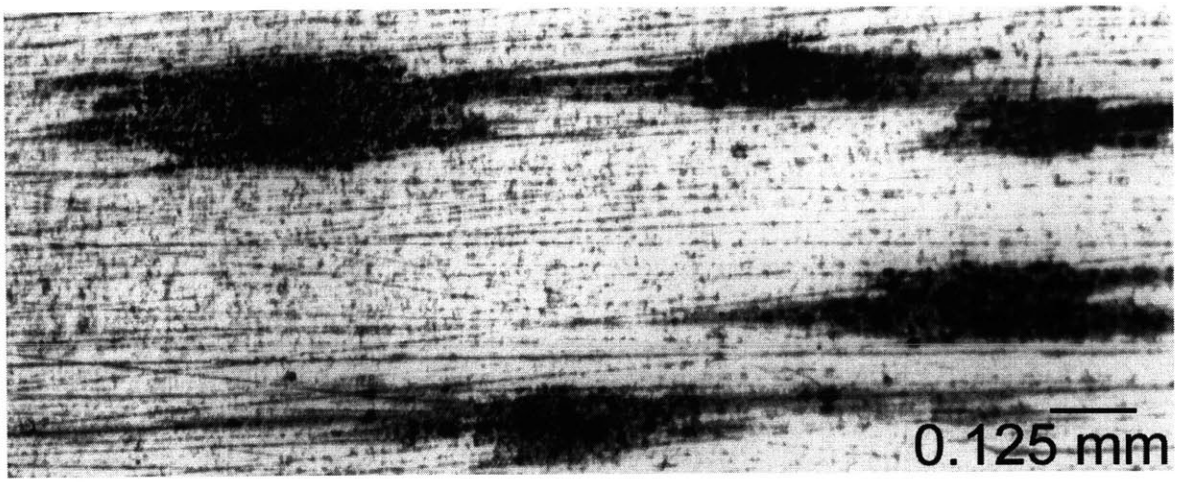

Figure 2-20: Underfilm Corrosion Initiating in Surface Defects

was viewed with an Olympus BX60M microscope at a magnification of 50x. These scratches provided a localized crevicelike environment in which corrosion could begin. A closer look at the underfilm corrosion is shown in Figure 2-21. This was taken on the confocal laser scanning microscope with a lens magnification of 50x. There is a central figure that protrudes from the surface of the sample. It was measured at a height of approximately 11.15 μm with respect to an uncorroded part of the surface. The two vertical dashed lines give the diameter, 91.365 μm, of the protrusion.

The impedance spectra for this foil sample can be seen in Figure 2-22. Both the Nyquist and the Bode plots are shown. Measurements were made initially, at time 0, after 1 hour, after 3 hours, and after 24 hours. This last measurement was after the corrosion was optically visible. The complex plane plot does not include the initial measurement because the scatter is so great due to the high impedance, as seen in the capacitive line in the modulus plot. The phase diagram shows the appearance of the second time constant, after a few hours.

Coated foil samples were then run for approximately 12 days in the more aggressive acidified solution. The initial spectra revealed both the polymer coating and the metal substrate, thus breaching the polymer was rather quick. With time the R_p values of the system decreased, thus the corrosion rate was increasing, but it none the less

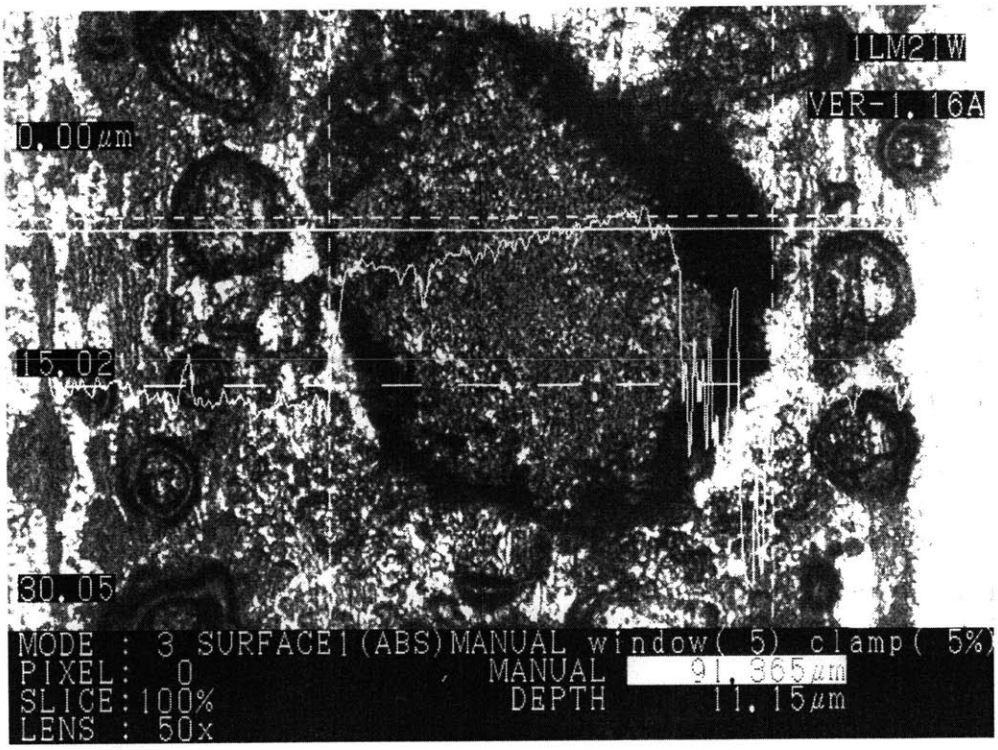

Figure 2-21: Underfilm Corrosion, Close-up

resulted in a mass loss too small to detect.

The samples themselves showed dark brown semi-circular regions with scale-like black flecks on the metal surface. In the middle of these regions blisters in the polymer were visible. On the sample presented in Figure 2-23 there is a pinkish colored blister. This is possibly a collection of corrosion products trapped by the polymer. The sample was viewed with a Bausch and Lomb stereo microscope, with a magnification of 10x and photographed with a Polaroid Microcam camera. The arrow indicating the blister also serves as the scale mark, the arrow corresponds to 0.53 mm. The edges of the darker corrosion region show thin lines of corrosion in the polishing scratches on the surface of the sample. This blister is clearly a region of delamination.

From the potentiostatic measurements performed previously on both the foil and wafer samples, it was decided that the amount of metal being lost by the foil would not be sufficient to carry out the EIS measurements in a timely manner. The wafer samples, however, could lose significatly less material and still be detectable with

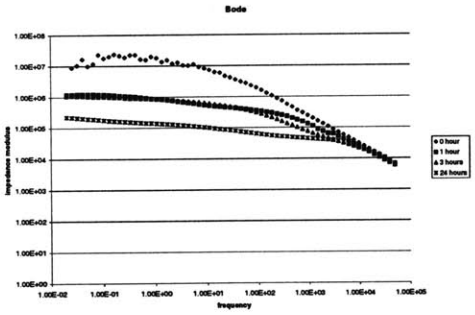

(Bode Modulus)

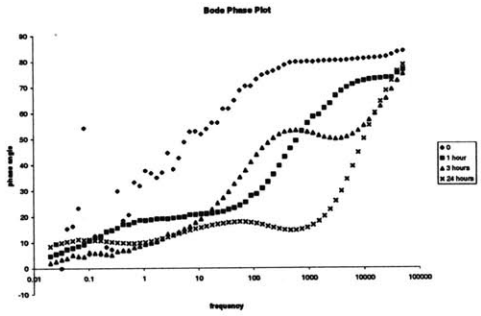

(Bode Phase)

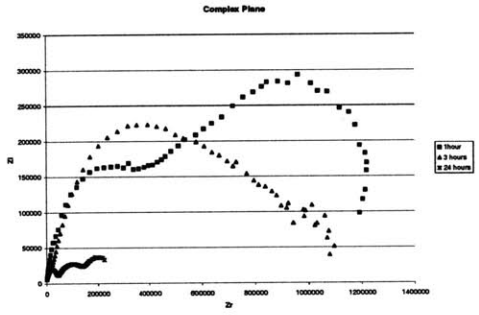

(Complex Plane)

Figure 2-22: Coated Cobalt Foil Impedance Spectra

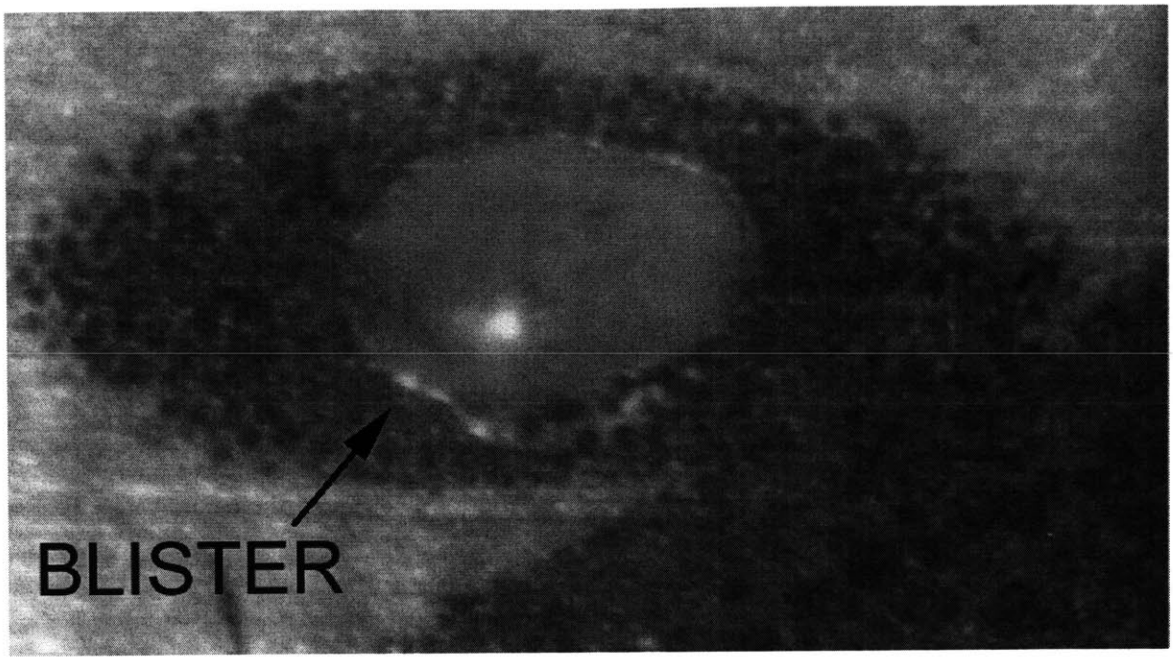

Figure 2-23: Sample Exhibiting A Blister

the magnetic technique, which will be discussed in length in the next chapter. The starting amount of cobalt is less, thus losing 2% of the wafer sample involves considerably less material than losing 2% of the foil sample. The wafers would need to lose something on the order of 5 μg, while the foils need to lose about 3 mg. Thus the acrylic coated wafers were the next system studied with EIS. The polyimide coating is a much better coating than the acrylic, so it was not studied for this project. The previous work conducted on this polymer indicated a lengthy time before the appearance of the second time constant [38].

Chapter 3

Magnetics

3.1 Ferromagnetism

The motion of electrons in a material causes magnetic behavior. Generally, this is rotation in orbits or spins which produces a magnetic field. This field effect is the magnetic moment of the spin or orbit [39]. In 1907, Weiss proposed that materials were composed of many regions which were each magnetized to saturation in some direction [40]. These regions are today known as domains. These domains derive their magnetic character from the orientation of the atomic magnetic moments, governed by the exchange energy, a function of the ratio of atomic separation to the diameter of unfilled electron shells [41]. These regions are magnetized to saturation with random directionality, thus the net magnetization of the material is zero [5]. Bloch hypothesized that the domain moments change through rotation, the direction of magnetization of the domain, and/or moving boundaries, a change in the volume of the domain [40]. Magnetizing a material is thus aligning the domain magnetizations in a single direction.

Materials generally fall into three categories—diamagnets, paramagnets, or ferromagnets. Diamagnetism consists of elements with an even number of electrons and complete inner shells, and no permanent magnetic moment. In the presence of a magnetic field these materials orient perpendicular to the field. Paramagnetism consists of elements with an odd number of electrons, a permanent magnetic moment, but

large interatomic spacing resulting in negligible atomic interaction. These materials orient parallel to the magnetic field. Ferromagnetism arises when there is a strong atomic interaction, the moments of neighboring atoms are aligned parallel and in the same direction. This interaction is between s and d electrons or s and f electrons. There are three characteristic behaviors of ferromagnets [5]: the magnetization curve approaches saturation, hysteresis occurs when the field is reversed, and there exists a temperature, the Curie temperature, above which the behavior becomes paramagnetic.

3.2 Properties and Hysteresis Loop

There are two basic magnetic quantities which when linked together yield a constant. From these three properties, all other magnetic properties can be derived [39]. These are, the magnetizing force or field, also called intensity (H) and the magnetic flux density or magnetic induction (B). The relationship between these two quantities is

$$B = \mu H \tag{3.1}$$

The constant μ is permeability, and frequently is unitless. It is defined as the ratio of the magnetic induction to the magnetizing force in a vacuum. Permeability can be used as a means of classifying materials. It is a constant of matter and characteristic in a given medium. If $\mu > 1$ it is paramagnetic, if $\mu < 1$ it is diamagnetic and if $\mu \gg 1$ it is ferromagnetic.

Susceptibility, k or χ, is the difference in the permeability of the materialrelative to the permeability of free space, a vacuum. A negative susceptibility is characteristic of diamagnets while a postive susceptibility is characteristic of paramagnets.

A magnetization curve shows the relationship between H and B. A characteristic of ferromagnetism is having a nonlinear curve, which is demonstrated by a hysteresis loop. There are several important points on this curve. When the magnetizing force is reduced to zero, the flux density lags behind and results in a residual flux, B_r, the

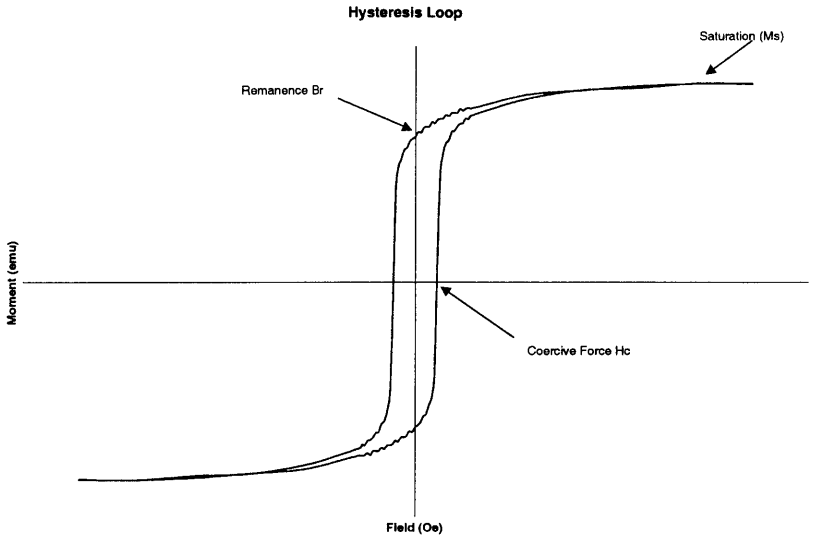

Figure 3-1: Magnetic Hysteresis Loop

remanence. The coercive force, H_c, is then the magnetizing force necessary to reduce the flux density to zero. The hysteresis or energy lost is attributable to domain wall motion. A ferromagnetic hysteresis loop is shown in Figure 3-1. Also shown on the loop is magnetic saturation, M_s, which is the limit of a magnetic moment for a ferromagnetic material. This is specific for the material. Despite increasing the field, once saturation is reached the moment will not increase further. The first time a magnetization curve is performed on a material that was not saturated prior to measurement, it will display what is known as a virgin curve in the first quadrant. This curve would fall within the loop shown in Figure 3-1 and join the loop as it neared saturation. If repeated loops are performed the subsequent loops will all follow the same path, which is different from the virgin loop path. When properties are reported, they are usually for the non-virgin loops, unless stipulated.

Magnetic properties can be split into two categories, structure insensitive and structure sensitive [5]. The structure insensitive properties consist of saturation,

the Curie temperature, magnetostriction, and anisotropy. The Curie temperature, θ_C, is the temperature where ferromagnetic materials begin to exhibit paramagnetic behavior. Above this temperature, there is disorder in the structure of the domains and the magnetic moments are no longer parallel to each other. Magnetostriction refers to a few different things: the Joule effect, a change in length of a ferromagnetic rod placed in a longitudinal magnetic field, the Guillemin effect, an elastically bent rod straightens in a longitudinal field, the Wiedemann effect, a rod twists while carrying a current if subjected to a magnetic field, and the Villari effect, a change in induction occurs when a magnetized rod is under longitudinal stress [5]. Anisotropy allows for directions of easy and difficult magnetization. Thus, there are different magnetization curves when a material is magnetized along different crystallographic directions. A lower energy, and thus, a lower field is required to saturate in the easy direction. The excess energy necessary to saturate the difficult direction is referred to as the anisotropic energy. The structure sensitive properties are permeability (not absolute), coercive force, and remancence. These properties are affected by strains, impurities, grain size and order-disorder transitions within the material.

3.3 Cobalt

Cobalt is an element of the transition group VIII between nickel and iron on the periodic table. These three elements along with gadolinium make up the ferromagnets. Structurally, at room temperature cobalt takes the form of a hexagonal close-packed system, ε. In this structure, the direction of easy magnetization is the [0001], or the c axis, and the $[10\bar{1}0]$ is the difficult direction. This leads to strongly uniaxial magnetic properties [42]. Thus the magnetization depends on the orientation of the applied field with relationship to the crystallographic axes. When the field is parallel to the easy axis, it is easier to reach saturation. Cobalt has a very high crystal anisotropy which affects the single crystal coercivity, as it is difficult to draw the magnetization of a domain away from it's direction [41]. In addition, high fields are required to saturate cobalt, on the order of 15,000 Oe [42].

Property	Value
Structure Insensitive	
saturation magnetic moment ($\frac{moment}{gram}$)	161
saturation magnetic moment ($\frac{moment}{cm^3}$)	1422
intrinsic saturation, M_s (G)	17,900
curie temperature, θ (^{o}C)	1121
crystalline anisotropy, K_1 ($\frac{ergs}{cm^3} x 10^{-6}$)	-0.051
saturation magnetostriction, λ_{100} (x10^{-6})	-46
saturation magnetostriction, λ_{111} (x10^{-6})	-24
Structure Sensitive	
hysteresis at saturation ($\frac{\frac{ergs}{cm^3}}{cycle}$)	2000
coercive force (Oe)	10
electrical resistivity (μohm-cm at 20 ^{o}C)	6.24
maximum permeability, μ_{max}	250

Table 3.1: Magnetic Properties of Cobalt

Cobalt is the most stable magnetic element. The Curie temperature is 1121 °C. This is the highest of all the ferromagnets. The ferromagnetic behavior will disappear when the magnitudes of the exchange energy and the thermal energy are equal. The magnetic saturation, or intrinsic induction, of cobalt is about 17,900 Gauss, this figure can vary depending only on the purity of the material that is used. Some magnetic properties of cobalt are listed in Table 3.1, the structure sensitive values are for commercially pure cobalt.

Another important part to the magnetics of cobalt, is the magnetics of its oxides. Since, for this research project the magnetics measurements are to be used to detect mass loss due to corrosion, the signal from the oxides must not interfere with the signal of the cobalt. The oxides CoO and Co_3O_4 are believed to be paramagnetic by most, however some researchers have reported that CoO is antiferromagnetic [40]. There is considerable debate over this in the literature, as there appears to be convincing arguments on both sides [40]. The only oxide of a ferromagnet that is known to have a strong magnetic signal is that of iron, the ferrites. In any case, the signal of the bulk cobalt is so much greater than that of any minute amount of oxide, such that measurements only reveal the bulk signal.

3.4 Measurement Instrumentation

There are three classes of typical methods to measure magnetic moments, and thus magnetic properties [43]. The first measures the force experienced by a material in a nonuniform magnetic field. The second measures the magnetic induction around a sample, such as monitoring voltage changes induced by a flux change when an external field is applied. Lastly is an indirect measurement of phenomena involving magnetic properties. The force method is difficult to use when measuring magnetization in a uniform field or when studying anisotropic materials. The indirect techniques available measure the Hall effect, Faraday effect, or resonance measurements. But since these are indirect methods, they are limited by the individual phenomena measured.

3.4.1 Vibrating Sample Magnetometer

A vibrating sample magnetometer, (VSM), measures the magnetic moment of a sample by vibrating it in a magnetic field. It was developed at MIT's Lincoln Laboratories by Dr. Simon Foner [44] and belongs to the second class of instrumentation that monitors induction. A VSM uses magnetic flux detection and depends on the sample motion to discriminate between the background flux and field distortion due to the sample [45].

The VSM vibrates the sample perpendicular to the applied field as demonstrated in Figure 3-2 [43]. A loudspeaker assembly, labeled vibrator assembly in the diagram, vibrates the sample rod on which the sample is attached. An induced voltage occurs in the stationary detection coils due to the magnetic field of the sample. Another set of detection coils, the reference coils also experiences a voltage, but induced by a reference sample attached to the drive rod. The vibrating frequency of the reference and the sample are the same, thus the voltages can be related to one another, resulting in a measurement of the magnetic moment of the sample. [43]

An important issue in the accuracy of the measurements is the position of the sample with respect to the reference coils [46]. An optimum position for the sample in 3-D space where the signal is independent of small displacements in location can

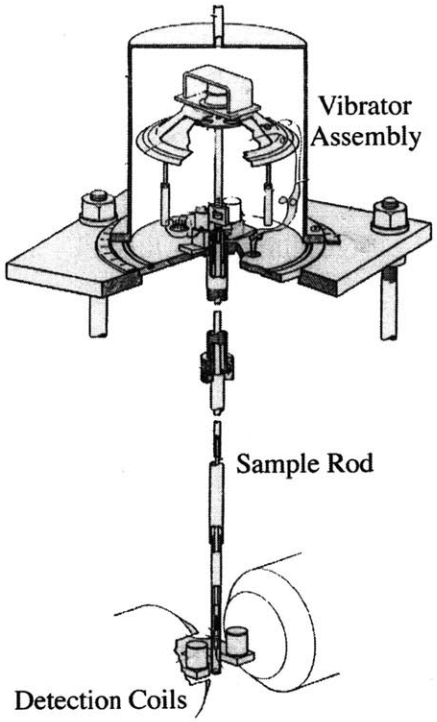

Figure 3-2: Diagram of VSM

be found. This is termed the saddle point, and is dependent on the number of detection coils and their configuration. There exist a number of different yet useful coil arrangements, generally an even number of coils is optimum.

The magnetometer must be calibrated. To do this, a standard reference comparison material is substituted for the sample. Generally the standard is a sample of pure nickel of known mass, the choice of standard is due to the low field that can be used to saturate nickel [43] [47] as well as the chemical stability and availability in high purity. The voltage gain can be adjusted so that the moment is standardized for the nickel reference.

The limits of sensitivity are a concern when using a VSM. These can be defined by the signal to noise ratio at the input circuit [43]. Much of the noise can be attributed to the Johnson noise of the pickup coil wire and the magnetic signal of the sample holder. To avoid a large sample holder signal, a weakly diamagnetic material of as little mass as possible is utilized [43]. Or a sample holder that appears to be semi-

infinite with respect to the coil diameter and is along the axis of symmetry should not induce a moment [46].

Another concern with the VSM is that of sample size. The optimum sample size and geometry is that of an ellipsoidal or spherical sample of relatively small size when compared to the detection coils [46] [48]. However, it is not possible for a research sample to conform to these requirements, so certain adjustments must be made. Again it is critical that the sample be at the saddle point in the field. The sample should not stray from the axis of symmetry by more than 0.1 of the sample's largest dimension [46]. If the sample dimensions are kept small with respect to the radius of the pickup coils, then regardless of geometry it may be approximated as a point dipole, which makes interpretation of the data the most straight forward [48].

3.4.2 Magnetics and Corrosion

There are a number of uses for magnetics testing, however, using magnetics to assess corrosion is a novel combination. In the recording industry, there have been numerous studies on the corrosion of magnetic films or magnetic tapes, and a number of other studies have been performed on the effects of oxide addition on magnetic properties. One of these studies [49] found that cobalt oxide, CoO, increased the coercivity and squareness of a magnetic media when added to it. This was determined to be due to how it affected the structure of the media, rather than the magnetic properties of the oxide itself. Another study indicated that magnetization–thickness products changed after corrosion of a sample [50]. In this study, the authors looked at corrosion rates as the ratio

$$\Delta M_s / M_s \tag{3.2}$$

This rate was then compared with other levels of relative humidity and absorbed water. Some other work done indicated a linear relationship between a change in magnetic saturation and mass loss of the samples [6].

Magnetics has also been used in corrosion detection. Since corrosion is an elec-

trochemical process which involves current flow, a magnetic field is generated. The magnitude of this field is proportional to the corrosion current intensity [51]. Thus the field generated can be used both to indicate the presence of corrosion, as well as studying electrochemical noise, interfacial impedances, and cyclic voltammetries [52].

3.5 Experimental Setup

This research furthers the study of the relationship of magnetic saturation, mass loss, and corrosion rate [6] [50]. Hysteresis loops were generated for cobalt samples both before and after various electrochemical tests were performed on them.

3.5.1 Samples

The samples used were of two types. The first was a 0.25 mm thick cobalt foil of 99.95% purity with an as-rolled finish, from Alpha Æsar. This foil was then cut into approximately 1.2 by 1.5 cm rectangular samples. This size was chosen to optimize the upper size limit of the detection coils of the VSM as well as to provide sufficient surface area for corrosion studies. Both bare and acrylic polymer coated samples were produced from these foils.

The second sample type was a silicon wafer with an e-beam deposited cobalt layer of a thickness of 3200 Å. These samples were made at the Microsystems Technology Laboratory at MIT. These samples were sectioned, using the technique outlined in the previous chapter, either into rectangular samples of approximately 2 by 4 cm or into samples the same size as the foils. The larger size is utilized with a larger, custom-made coil configuration for the VSM. Wafers were either coated at MTL with a polyimide or in-house with an acrylic polymer.

3.5.2 Equipment

All magnetic measurements were carried out with a Model 880 vibrating sample magnetometer from Digital Measurement Systems, Inc. This VSM is shown in Figure

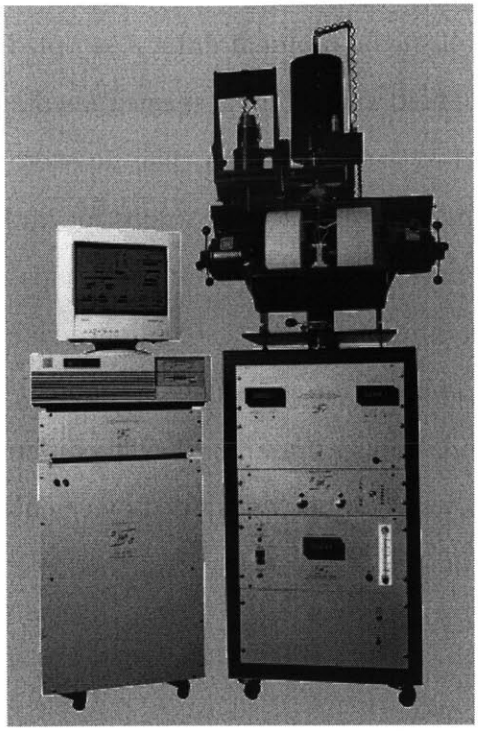

Figure 3-3: DMS Model 880 VSM

3-3. The instrumentation is controlled by a computer measurement system written in Visual BASIC and capable of measuring all of the basic magnetic properties as well as performing some more advanced techniques [53]. A cooling system can be seen next to the VSM, this is connected as a closed system with the VSM to prevent overheating. The VSM was selected as the testing method due to the level of sensitivity and reproducibility of the measurements, the ability to use different sizes and geometries of samples, and the relative ease with which measurements can be made.

The VSM has two different pole cap configurations. The standard set incorporates 2 inch diameter tapered pole caps, which can reach fields up to 18,500 Oe. A set of custom coils was also used, these have a 4 inch diameter non-tapered pole cap, and fields up to 8000 Oe can be obtained [53]. The pole gap, the distance between the poles where the sample is located, can be adjusted. The smaller the pole gap, the larger the possible field, thus maximum fields previously mentiond can not be obtained at wide pole gaps.

When generating hysteresis loops, the sample is first brought to saturation, to

avoid virgin curves. To collect the moment data, a sampled measurement technique is employed. This allows the field and moment measurements to settle before continuing to sweep. Each individual measurement can then be averaged to reduce noise [53].

The VSM has three different adjustment knobs for finding the saddle point. One each for the x, y, and z axes. With the small pole caps, the z and the y axes are maximized, while the x is minimized, the axes follow a right hand coordinate system, with z the vertical axis. The custom coils have a different saddle point, with both y and x being minimized and z being maximized. This difference is due to the different configuration of the poles, and can be determined by calculating a sensitivity function for the geometry of the coils [46].

3.6 Results

Over 900 loops were generated using cobalt samples. The behavior associated with the foil and wafer samples was slightly different. The main difference between the two types of samples is the field necessary to reach saturation. This is apparent in Figure 3-4. The relative moments of the samples at saturation are different, this is due to the amount of cobalt present in the samples. The field to reach saturation for the foil is about 14,000 Oe, while for the wafer it is about 4,000 Oe. This is due to the structural differences of a sputter deposited film of metal and the metal in the bulk form. All of this stems from the anisotropy and directionality of cobalt. The structure of the thin film is influenced by the electrodeposition technique. This technique split the metal on an atomic scale before it was precipitated [54]. The structure of the thin films is such that less energy is required to achieve saturation, thus a lower field is necessary. The coercivity of the thin film is greater than that of the bulk cobalt. This is due to the fact that the grains are so small that these grains approach a single magnetic domain in size, thus there are few domain walls. Wall movements are easier to achieve than rotation of magnetization, but in thin films the change in magnetization can only be realized through this rotation. Thus more energy is required for rotation and the coercivity is greater [54]. This is evidenced in

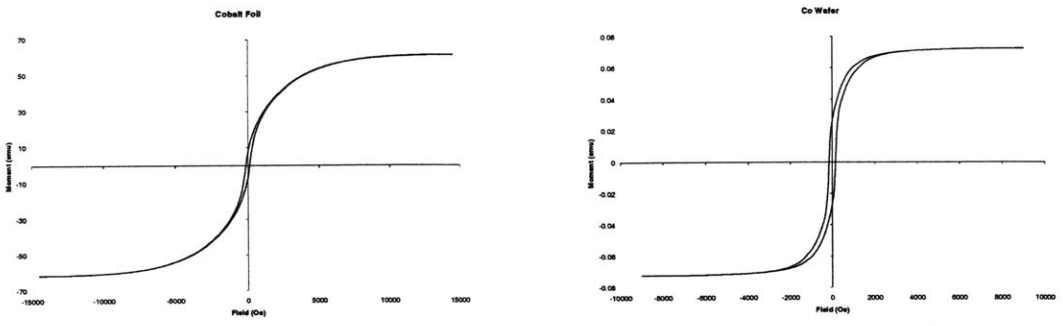

(Foil Hysteresis Loop) (Wafer Hysteresis Loop)

Figure 3-4: Comparison of Cobalt Foil and Wafer Hysteresis Loops

Figure 3-4 by the greater slope of the wafer sample.

The standard reference sample used during calibration was a nickel disc with a moment of 3.475 emu. The sample holders were either 3 mm diameter Pyrex glass tubing or a 5 mm diameter plexiglass rod. Measurements of the sample holder were made as part of the machine calibration to be subtracted from the resulting data, which also subtracted the ambient noise. The pyrex rod has a very small signal which is barely detectable while the plexiglass rod has a slightly greater signal. This signal was measured as diamagnetic and at least two orders of magnitude smaller than the smallest cobalt signals being recorded.

Hysteresis loops for the foils were run from 14,500 Oe to -14,500 and back. The wafer loops were run from 8,000 Oe to -8,000 Oe and back. Starting the measurements at a field beyond saturation eliminated the virgin curve. The moment at each point was averaged 25 times during the measurement, and more data points were taken in the region of saturation than the rest of the loop; however, attention was also paid to the intercepts of both axes, the coercive force and the remanence, as well.

Hysteresis loops were generated both before and after samples were corroded. A number of runs were performed at each time and the saturation values were averaged. Generally between 6-10 measurements were made yielding a deviation on the order of 0.04–0.29 emu. This is small compared to the change in saturation resulting from corrosion.

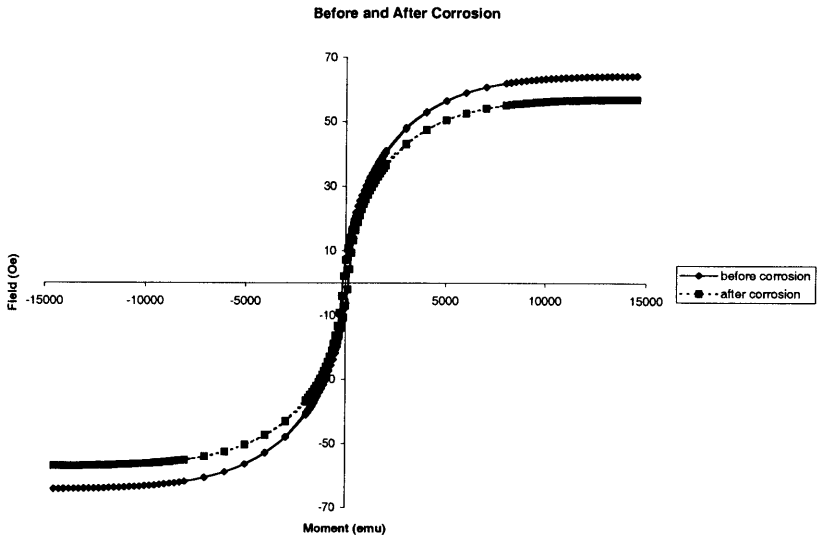

Figure 3-5: Decrease in Saturation After Corrosion

An example of the change of magnetic saturation due to corrosion can be seen in Figure 3-5. These results are for a bare cobalt foil sample that was corroded during a potentiostatic test. The change in saturation is 11.12 % , and was compared with the mass loss of the sample, which was weighed before and after the corrosion. Figure 3-6 shows the results of a number of samples with the % change in saturation plotted as a function of the change in mass loss determined with a balance. The curve is linear with a slope of one. The equation for the trend line is $y = 0.9999x$ with an R^2 value of 0.9918. Changes on the order of 1% were detectable–this is the detection limit of the instrument as communicated by DMS. The same set of measurements were also carried out on cobalt wafer samples with similar results. It should be mentioned that a smaller amount of mass loss could be detected for the wafer samples than the foil samples. There is less magnetic material in the wafer samples than in the foil samples, thus a 1% loss of wafer mass is considerably smaller than a 1% mass loss of foil. This smaller mass loss still corresponds with the same correlation to the

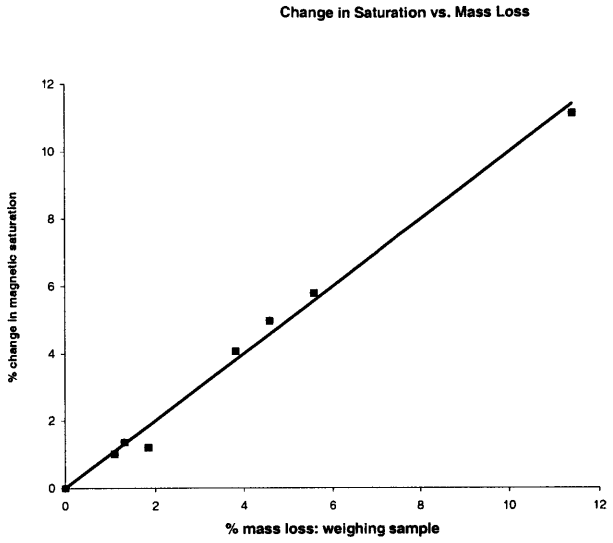

Figure 3-6: Comparison of Saturation Change and Gravimetric Mass Loss Data

magnetic saturation change. Thus, while it is possible to detect a loss of material on the order of 5 μg for the wafer samples, a much greater loss is required for the foil specimens.

It is interesting to note that when a sample is coated with the polymer, there may be a small change in the magnetic saturation. The cause of this change is unknown. One possibility is related to the magnetostrictive effect that cobalt experiences. When cobalt, and other ferromagnetic materials, are subjected to a stress, there can be a slight change observed in the magnetic behavior [5]. For the samples used in this study, however, this does not seem to be supported by the fact that the stress applied on one side of the cobalt foil due to the coating is somewhat balanced out by the stress due to the coating on the other side of the sample. In addition, there is no observed difference in effect when a comparison of different coating thicknesses is made. Further, the effect of magnetostriction should be reversible. When the stress is removed, the system should return to its prior state. That was not the

case when samples in this study were subjected to an acetone strip—the saturation measurement did not return to the original. To circumvent this problem, the magnetic measurements were made after the coating was applied, then a known amount of material was removed, and the subsequent saturation change was noted. This change agreed with the mass loss in the same fashion as the information reported in Figure 3-6. Thus it was concluded that it is okay to measure the mass loss of a coated sample when the initial measurement is taken of the complete, coated system. And the concern of trapped corrosion products in the polymer affecting the magnetic measurements was addressed earlier—cobalt oxides are not ferromagnetic and do not have strong magnetic signatures, there is even doubt as to in which magnetic class they belong.

Chapter 4

Correlation of Electrochemical and Magnetic Techniques

The past two chapters have explored the two very different fields of study, electrochemistry and magnetics, used during this project. The electrochemical and magnetic tests performed are not unusual; however, joining the two techniques to assess corrosion is unique. Corrosion studies on magnetic materials have been studied, and with it the change in their magnetic properties, but evidence of using magnetic techniques to quantify mass loss and corrosion rate, was not found in the literature.

4.1 Combination of Data from All Techniques

The results shown in Figures 2-14 and 3-6 indicate that both the electrochemical mass loss data and the magnetic saturation data have a linear 1:1 relationship with the gravimetric mass loss data. These two plots can be combined to yield Figure 4-1. The trend line has an equation $y = 0.9922x$ and an R^2 value of 0.9907. Here the electrochemical mass loss is compared with the magnetic saturation change. The correlation is, as expected from the other two figures, linear with a slope of one. This allows for using the two forms of data directly, without the intermediate step of weighing and re-weighing the samples. This is also useful in situations where it is not possible to weigh a sample, such as a polymer coated system. In this case the

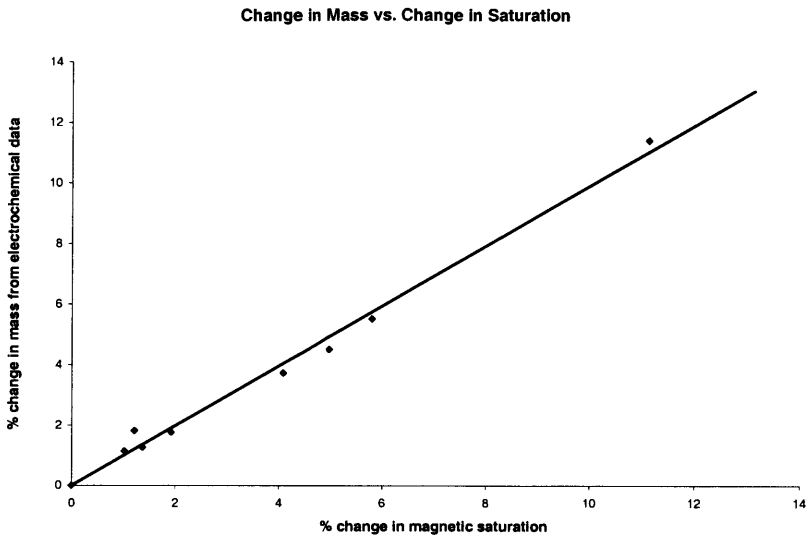

Figure 4-1: Comparison of Magnetic Saturation Change and Electrochemical Mass Loss

polymer absorbs water and the corrosion products are trapped on the surface, thus affecting the gravimetric mass loss measurements.

A comparison of all three, the electrochemical, the gravimetric, and the magnetic information is presented in the bar plot in Figure 4-2. The data for 8 cobalt foil samples are presented. The names of the samples are purely for cataloging purposes and do not represent anything else. The wafer samples yielded a similar relationship, not shown here, between the electrochemical and magnetic techniques. The actual mass of the cobalt deposited on the wafer could not be directly measured since it was part of a composite system and the mass loss incurred is less than 1 mg. The accompanying data for the bar graph is presented in Table 4.1. It should be noted as a reminder that the electrochemical data presented here is from potentiostatic and potentiodynamic testing. Each foil sample was weighed and also tested on the VSM. It subsequently underwent aqueous corrosion and was then re-weighed and retested in the VSM. Both before and after an experiment, 6-10 hysteresis loops were run for each

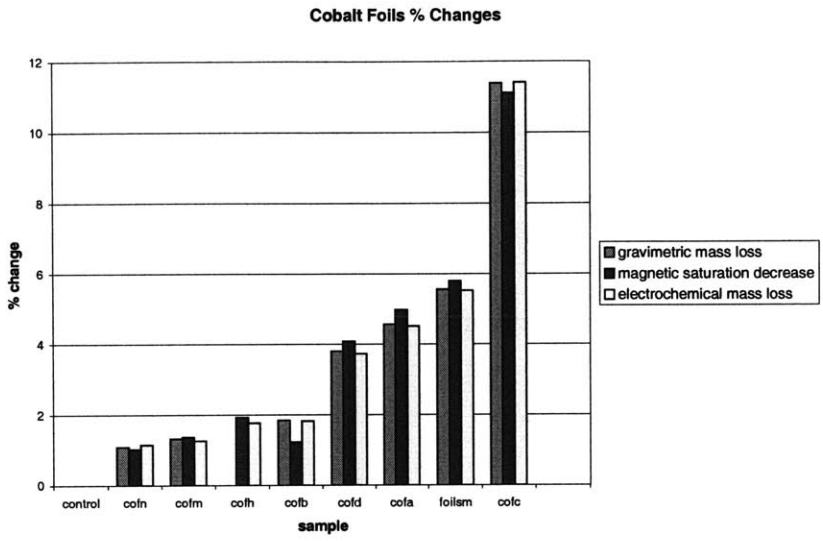

Figure 4-2: Comparison of All Three Techniques

sample. The range of mass loss and saturation decrease is between 1–11%. Sample cofH does not have a gravimetric data point because the initial mass was recorded before a wire was attached, thus the final mass could not be accurately determined for just the cobalt foil since it was weighed as a complete system.

The initial EIS results could not be compared with any magnetic results because the amount of mass loss was below the tolerance of both the balance and the VSM. These tests were performed on cobalt foil samples. Preliminary results for the cobalt wafer samples indicate that using the wafers will accomplish the goal of this project. After running a sample for 13 days in 0.5 M NaCl a 19.6% change in magnetic saturation was detected. This corresponds to about 180 μg of cobalt.

Sample	Gravimetric Mass	Electrochemical Mass	Magnetic Saturation
CofA	4.57	4.51	4.98±.31
CofB	1.84	1.81	1.22±.27
CofC	11.39	11.41	11.12±.16
CofD	3.81	3.73	4.08±.30
CofH		1.77	1.92±.26
CofM	1.31	1.26	1.37±.16
CofN	1.09	1.14	1.02±.15
Foilsm	5.56	5.52	5.79±.21

Table 4.1: Data for Comparison of All Three Techniques, in % Change

4.2 Error

The error of the three different measurements is dependent on the technique used. The gravimetric data was gathered on a Mettler balance with readability to 0.1 mg. Determination of the starting mass of the wafer samples, something necessary for determining the % change in mass loss, was done by measuring the surface area as accurately as possible and then using the volume and density to find the mass. The density used was 8.86 $\frac{g}{cm^3}$. A problem with this method is that the sputtered cobalt has some oxide content and the density is not the same as the bulk density used in the calculations. The electrochemical data is an integration under an experimental curve, it is affected by the measurement capabilities of the potentiostat. During the open circuit potential measurements there could be very minute amounts of mass lost, but these are not taken into account. The sample cell arrangement was also important. The electrochemical setup involved two separate vessels connected through a solution bridge. As stated earlier, the location of the Luggin probe tip with respect to the working electrode can affect the data, because the ohmic resistance of the solution is minimized only when the tip is at an optimum distance. The magnetic measurement error is measured as the deviation between runs, the reproducibility, and was determined to be in the range of ±.04–±.30 emu. This value is much smaller than the moment changes being detected as a result of corrosion. And these errors can be attributed to user error, slight deviation from the saddle point, and temperature

fluctuations in the vicinity of the VSM. Magnetic properties are temperature dependent, and all numbers reported here were measured at room temperature; however, the VSM is not temperature controlled, and is thus susceptible to changes in temperature. For cobalt, the manifestation of effects in the data due to small temperature fluctuations around room temperature is fairly small. To counter this source of error, the VSM was calibrated between each run. Since this entailed removing the test sample and replacing it with the nickel standard, when the sample was returned, the saddle point had to be redetermined. There is a region in space around the saddle point where the error due to positional deviation is negligible, but outside that region it increases dramatically [46]. Consequently, small deviations from the saddle point as a result of recalibration were not considered to be significant relative to the drift of the machine. The drift, which is combatted with calibration between each run, can be attributed to the temperature effects mentioned previously, the VSM heating up with use—as the wires and connections heat up they produce more noise that can be detected by the coils. In addition, different fields generated by other equipment in the laboratory may have some minor effect.

Chapter 5

Conclusions and Future Work

Before any testing could be performed on the polymer coated metal systems, the behavior of the bare metal system needed to be understood. The corrosion behavior of bulk cobalt and thin film cobalt deposited on a silicon wafer was studied. The tests performed to asses this were potentiodynamic and potentiostatic scans. Since this project had an objective that encompassed two different testing methods, the basic magnetic properties of the cobalt had to also be assessed before further work could be conducted. These tests involved hysteresis loops generated in the VSM, and they revealed that the magnetic signal of the cobalt was sufficient to be detected clearly above the ambient noise and sample rod signal. It was also determined that the VSM was sensitive enough to measure small changes in magnetic saturation, on the order of 1%.

With the preliminary testing complete, the bulk of the research was initiated. The cobalt foil and cobalt wafer samples were monitored for mass loss through three different testing techniques: gravimetric, electrochemical, and magnetic. The gravimetric results were assessed by weighing a sample before and after the sample was corroded. The electorchemical mass loss data was generated by integrating the current-time plot from the potentiostatic and potentiodynamic scans that caused the corrosion. Hysteresis loops were performed before and after the sample was corroded to measure the magnetic saturation change due to corrosion. The culmination of these sets of tests is the conclusion that the magnetic and electrochemical data correlate well

enough to use the two techniques in conjuction with each other and as a check for each other. The gravimetric data gave the extra confidence in the data taken here. Figures 4-1 and 4-2 show these results. The magnetic and electrochemical data can be represented as a linear curve with slope of one—thus a 1% change in magnetic saturation indicates a 1% change in mass.

Once this baseline curve for comparison of the magnetic and electrochemical data was established, the next phase of this project was started. The intention here was to correlate mass loss and corrosion rate with the electrochemical data using magnetics as the measurement device. Two different types of electrochemical tests were used: polarization resistance and electrochemical impedance spectroscopy. The polarization resistance was performed on bare metal samples. It monitored the open circuit potential of a sample while intermittently running a potentiodynamic scan ±30 mV around the corrosion potential. This was conducted for over 30 hours. Subsequent analysis of the data revealed the corrosion current with time which could be converted to corrosion rate and mass loss; however, the mass loss assessed from this data was determined to be too small to detect with the magnetic technique. This in fact turned out to be correct as the hysteresis loops showed no measurable change.

EIS tests were performed on coated cobalt foil samples. These tests are similar to the polarization tests in that they monitor the open circuit potential and then periodically perform a measurement. These periodic measurements, however, were an AC fluctuation of ±25 mV around the corrosion potential and data was recorded over a large frequency range. EIS data were collected for a sample for exposure times in excess of one week. The resulting data was analyzed to reveal various resistance and capacitance values which could be fit to an equivalent circuit. These results in of themselves were interesting in what they showed about the coated system of study, but the R_p values were not low enough to indicate a corrosion rate great enough to lose an amount of metal sufficient to be measurable in the VSM. Again, runs were made in the VSM, to determine if the mass loss could be detected, but it could not. One of the parameters of the system needed to be changed. One good thing about these tests, however, was that the magnetic and the electrochemical results showed

mass loss levels below 1% of the total.

The sample system under evaluation was the first parameter altered. Instead of using the cobalt foils, the wafer samples were used. These samples had less cobalt to begin with, thus less metal had to be lost to detect a 1% change. Despite the promising work here, more samples need to be tested so enough reproducible data is generated. Results from preliminary experiments indicate that the mass loss from corrosion by EIS is detectable in the VSM.

The important initial baseline comparison between the electrochemical and magnetic techniques was firmly established. Further work is currently being done to apply these findings to the coated system studied by electrochemical impedance spectroscopy. Now that an understanding of the length of time, aggressivness of the solution, and sample type has been reached, the electrochemical testing should proceed as smoothly as any research can. It is anticipated that the results of the EIS and VSM data will correlate as nicely as those of the bare metal.

The wafer system being studied by EIS right now is the acrylic coating. The polyimide samples will also be studied. In the future, it is hoped that other polymers, perhaps relevant to different industries, will be used too. These other polymers would behave differently in the solution, bond differently with the substrate, and have varied defect densities due to application. All factors that affect the evolution of the underfilm corrosion observed.

Work is also underway to perform in-situ EIS experiments in the VSM. This would permit the sample to be subjected to an EIS run and then immediately generate a hysteresis loop. The preliminary work on a cell design to allow both forms of testing is being done, as well as the initial magnetic studies of the cell with and without cobalt in it.

To better understand the underfilm corrosion, it is necessary not only to measure the corrosion and the polymer behavior through electrochemical means, but also to characterize the interface of the metal/polymer. This was initiated recently, resulting in Figure 2-7. That sample was fractured in liquid nitrogen and then imaged in an SEM. The original intention was to use ultramicrotomy to produce thin sections for

examination in the TEM. The wafer samples shattered when subjected to the diamond knife, and thus another method had to be found or developed. Ultramicrotomy is possible for the cobalt foil samples, however, and that is currently being done. Both the polyimide and the acrylic samples will be examined. A result of this assessment could potentially lead to a surface preparation of the cobalt foils before application of the polymer. Currently the foils are left in their as-rolled state, which manifests itself as parallel scratches across the surface in the direction of the roll. Some believe this rougher surface allows for a better mechanical bond with the polymer, while others believe this impedes the binding. Perhaps examining the interface will resolve the issue for this particular system.

Another aspect of the coated system to be investigated in the future is the effect of defects. Introducing defects into the system at the interface would assist with the assessment of delamination. It is anticipated that defects deliberately introduced into the coating would decrease the time until the appearance of a second time constant, and the start of underfilm corrosion. This was done to a limited extent by undercuring the acrylic and adjusting the acetone content to affect fluidity. In the future this should be carried out through a more quantified and systematic approach.

Appendix A

List of Symbols

Symbol	Definition
M_s	Magnetic Saturation
E_{corr}	Corrosion Potential
η	Overpotential
β_a	Anodic Tafel Constant
β_c	Cathodic Tafel Constant
i, I	Current or Current Density
ϕ	Potential
$\Delta\phi$	Potential Change
I_{corr}	Corrosion Current
R_p	Polarization Resistance
V	Voltage
f	Frequency
ω	Angular Frequency
Z_{re}, Z'	Real (Resistive) Component of the Impedance
Z_{im}, Z''	Imaginary (Reactive) Component of the Impedance
$\mid Z \mid$	Modulus of the Impedance
Θ	Phase Angle
k	Boltzman Constant

Symbol	Definition
R_Ω	Solution Resistance
R_{po}	Pore Resistance
C_c	Coating Capacitance
C_{dl}	Double Layer Capacitance
ϵ	Dielectric Constant
d	Thickness of Coating
A	Area or Surface Area
F	Faraday's Constant
m	Mass
r	Rate
B	Magnetic Moment/Flux
H	Magnetic Field
μ	Permeability
k, χ	Susceptibility
B_r	Magnetic Remanence
H_c	Coercive Force
Θ_C	Curie Temperature
λ	Magnetostriction
K_1	Crystalline Anisotropy
V_t	Thermal Voltage
T	Temperature
τ	Time Constant

Appendix B

List of Abbreviations

Abbreviation	Definition
EIS	Electrochemical Impedance Spectroscopy
VSM	Vibrating Sample Magnetometer
MF	Melamine-Formaldehyde
PI	Polyimide
SCE	Saturated Calomel Electrode
SHE	Standard Hydrogen Electrode
DI	Dionized
AC	Alternating Current
DC	Direct Current
SEM	Scanning Electron Microscope
TEM	Transmission Electron Microscope
MTL	Microsystems Technology Laboratory
DMS	Digital Measurement Systems

Bibliography

[1] Mars G. Fontana. *Corrosion Engineering.* McGraw-Hill, Inc., New York, third edition, 1986.

[2] Denny A. Jones. *Principles and Prevention of Corrosion.* Prentice-Hall, Inc., Upper Saddle River, New Jersey, second edition, 1996.

[3] F. Mansfeld. Use of electrochemical impedance spectroscopy for the study of corrosion protection by polymer coatings. *Journal of Applied Electrochemistry*, 25:187–202, 1995.

[4] Florian Mansfeld. Tafel slopes and corrosion rates from polarization resistance measurements. *Corrosion*, 29(10):397–402, 1973.

[5] James K. Stanley. *Electrical and Magnetic Properties of Metals.* ASM, Metals Park, Ohio, 1963.

[6] D.B. Mitton. *Degradation of Thin Metal/alloy Films (for Magnetic Recording).* PhD thesis, UMIST, 1989.

[7] W. von Baeckmann, W. Schwenk, and W. Prinz, editors. *Handbook of Cathodic Corrosion Protection: Theory and Practice of Electrochemical Protection Processes.* Gulf Publishing Co., Houston, Texas, third edition, 1997.

[8] Werner Funke. Mechanism of protecting metals by organic coatings against corrosion. In Martin Kendig and Henry Leidheiser Jr., editors, *Corrosion Protection by Organic Coatings*, volume 87-2 of *Proceedings of the Symposium on Corrosion*, pages 1–10, Pennington, New Jersey, 1987. ECS Corrosion Division, ECS.

[9] Werner Funke. How organic coating systems protect against corrosion. In Ray A. Dickie and F. Louis Floyd, editors, *Polymeric Materials for Corrosion Control*, number 322 in ACS Symposium, pages 222–228. Oxford University Press, Washington, DC, 1986.

[10] Gordon P. Bierwagen. Corrosion and its control by coatings. In Gordon P. Bierwagen, editor, *Organic Coatings for Corrosion Control*, number 689 in ACS Symposium, pages 1–8. Oxford University Press, Washington, DC, 1998.

[11] Gordon P. Bierwagen, Dennis E. Tallman, Joel Zlotnick, and Carol S. Jeffcoate. Defects and heterogeneities in corrosion protective organic-coatings films and their effects on film performance. In Gordon P. Bierwagen, editor, *Organic Coatings for Corrosion Control*, number 689 in ACS Symposium, pages 123–136. Oxford University Press, Washington, DC, 1998.

[12] Walter Brockmann. Durability of metal polymer bonds. In K. L. Mittal, editor, *Adhesion Aspects of Polymeric Coatings*, New York, 1983. ECS, Plenum Press.

[13] D. E. Packman. The adhesion of polymers to metals:the role of surface topography. In K. L. Mittal, editor, *Adhesion Aspects of Polymeric Coatings*, New York, 1983. ECS, Plenum Press.

[14] Ray A. Dickie. Adhesion of organic coatings and its loss due to corrosion. In K. L. Mittal, editor, *Adhesion Aspects of Polymeric Coatings*, New York, 1983. ECS, Plenum Press.

[15] Henry Leidheiser Jr. Mechanisms of de-adhesion of organic coatings from metal surfaces. In Ray A. Dickie and F. Louis Floyd, editors, *Polymeric Materials for Corrosion Control*, number 322 in ACS Symposium, pages 124–135. Oxford University Press, Washington, DC, 1986.

[16] L.L. Shreir, R.A. Jaman, and G.T. Burstein, editors. *Corrosion*, volume 2, Corrosion Control. Butterworth Heinmann, Oxford, 1994.

[17] Syh-Ming Lian, K.M. Chen, and Aina Hung. Studies of polyimide/metal interface. *Journal of the Electrochemical Society*, 141(9):2374–2379, 1994.

[18] D. Wilson, H.D. Stenzenberger, and P.M. Hergenrother, editors. *Polyimides.* Chapman and Hall, 1990.

[19] D.B. Mitton, R.M. Latanision, and F. Bellucci. The effect of post-cure annealing on the protective properties of polyimides on chromium substrates. *Journal of the Electrochemical Society*, 143(10):3307–3316, 1996.

[20] F. Bellucci and L. Nicodemo. Water transport in organic coatings. *Corrosion*, 49(3):235–247, 1993.

[21] Zeno W. Wicks Jr., Frank N. Jones, and S. Peter Pappas. *Organic Coatings:Science and Technology*, volume 1 of *SPE Monograph.* John Wiley & Sons, Inc., New York, 1992.

[22] R. D. Armstrong, J. D. Wright, and T. M. Handyside. Impedance studies into the corrosion protective performance of a commercial epoxy acrylic coating formed upon tin plated steel. *Journal of Applied Electrochemistry*, 22:795–800, 1992.

[23] I.V. Pyatnitskii. *Analytical Chemistry of Cobalt.* Analytical Chemistry of Elements, Vernadskii Institute of Geochemistry and Analytical Chemistry USSR Academy of Sciences. Ann Arbor—Humphrey Science Publisher, Ann Arbor, Michigan, 1969.

[24] E. Betteridge. *Cobalt and Its Alloys.* Ellis Horwood Industrial Metals Series. John Wiley & Sons, New York, 1982.

[25] Wolfgang J. Lorenz and Konrad E. Heusler. *Corrosion Mechanisms*, volume 28 of *Chemical Industries*, chapter Anodic Dissolution of Iron Group Metals, pages 1–83. Marcel Dekker, Inc., New York, 1987.

[26] Marcel Pourbaix. *Atlas of Electrochemical Equilibria in Aqueous Solutions.* NACE, Houston, Texas, 1974.

[27] V. Brusic, G.S. Frankel, A.G. Schrott, T.A. Peterson, and B.M. Rush. Corrosion inhibition of cobalt with a thin film of Cu-BTA. *Journal of the Electrochemical Society*, 140(9):2507–2511, 1993.

[28] A.T. Kuhn and J. Wellwood. Aqueous and atmospheric corrosion of cobalt-nickel alloys. *British Corrosion Journal*, 21(4):228–234, 1986.

[29] ASTM. *Standard reference method for making potentionstatic and potentiodynamic anodic polarization measurements.* G5.

[30] W.J. Lorenz and F. Mansfeld. Determination of corrosion rates by electrochemical DC and AC methods. *Corrosion Science*, 21(9):647–672, 1981.

[31] M. Stern and L. Geary. Electrochemical polarization: A theoretical analysis of the shape of polarization curves. *Journal of the Electrochemical Society*, 104(1):59–63, 1957.

[32] M. Stern. Electrochemical polarization: Ferrous-ferric electrode kinetics on stainless steel. *Journal of the Electrochemical Society*, 104(9):559–563, 1957.

[33] J. Ross Macdonald, editor. *Impedance Spectroscopy:Emphasizing Solid Materials and Systems.* John Wiley & Sons, Inc., New York, 1987.

[34] Bernard A. Boukamp. A nonlinear least squares fit procedure for analysis of immittance data of electrochemcial systems. *Solid State Ionics*, 20:31–44, 1986.

[35] G.W. Walter. A review of impedance plot measurements used for corrosion performance analysis of painted metals. *Corrosion Science*, 26:681–703, 1986.

[36] Jeh-Beck Ju and William H. Smyrl. Corrosion studies of thin film materials for magnetic and microelectronic applications. In *Electronic Packaging and Corrosion in Microelectronics*, pages 119–129, Minneapolis, MN, April 1987. ASM.

[37] S. Frangini. Corrosion rate and anodic dissolution behvior of a B2-iron aluminide alloy in sulfuric acid. *Corrosion*, 55(1):89–95, 1999.

[38] Eddy Kong-Yiam Tan. Corrosion initiation studies of polyimide coated metallic substrates. Master's thesis, Massachusetts Institute of Technology, 1991.

[39] Raymond L. Sanford and Irvin L. Cooter. Basic magnetic quantitites and the measurement of the magnetic properties of materials. Monograph 47, National Bureau of Standards, Gaithersburg, MD, May 1962.

[40] Richard M. Bozoroth. *Ferromagnetism.* IEEE Press, New York, 1993.

[41] F. Anselin. Cobalt and magnetism. *Cobalt*, (12), 1961.

[42] R. Pauthenet. Magnetic properties of cobalt and of some cobalt alloys and ionic compounds. *Cobalt*, (26):3–9, 1965.

[43] Simon Foner. Versatile and sensitive vibrating sample magnetometer. *Review of Scientific Instruments*, 30(7):548–557, 1959.

[44] Simon Foner. Vibrating sample magnetometer. *Review of Scientific Instruments*, 27(7):548, 1956.

[45] S. Foner. The vibrating sample magnetometer: Experiences of a volunteer. *Journal of Applied Physics*, 79(8):4740–4745, 1996.

[46] A. Zieba and S. Foner. Detection coil, sensitivity function, and sample geometry effects for vibrating sample magnetometers. *Review of Scientific Instruments*, 53(9):1344–1354, 1982.

[47] Dieter Eckert and Johannes Sievert. On the calibration of vibrating sample magnetometers with the help of nickel reference samples. *IEEE Transactions on Magnetics*, 29(6):3001–3003, 1993.

[48] C. Johansson and M. Hanson. Influence of sample geometry in a vibrating sample magnetometer. *IEEE Transactions on Magnetics*, 30(2):1064–1066, 1994.

[49] R. Ranjan, M. Lu, T. Yumashitu, and T. Chen. Effect of cobalt oxide addition on Co-Pt media. *IEEE Transactions on Magnetics*, 30(5):3942–3944, 1994.

[50] H. Suzuki, Y. Shiroishi, S. Hishiyama, T. Ohno, Y. Matsuda, F. Matsunaga, and N. Tsumita. Magnetic properties and corrosion-resistance of sputtered Co-Ni films for longitudinal recording. *IEEE Transactions on Magnetics*, 23(5):3411–3413, 1987.

[51] J.G. Bellingham, M.L.A. MacVicar, M. Nisenoff, and P.C. Searson. Detection of magnetic fields generated by electrochemical corrosion. *Journal of the Electrochemical Society*, 133:1753, 1986.

[52] V. Poulbot, H. Glenat, N. Kernevez, F. Coulet, F. Dalard, and J.J. Raneau. Study of corrosion processes by magnetic measurements. In J.M. Costa and A.D. Mercer, editors, *Progress in the Understanding and Prevention of Corrosion*, pages 1463–1471. Institute of Materials, 1993.

[53] DMS Inc. Torque/VSM 880. web site.

[54] A. Dupré. Electrical and magnetic properties of thin cobalt films. *Cobalt*, (6):3–7, 1960.

[55] F. Mansfeld, S.L. Jeanjaquet, and M.W. Kendig. An electrochemical impedance spectroscopy study of reactions at the metal/coating interface. *Corrosion Science*, 26(9):735–742, 1986.

[56] F. Mansfeld, M.W. Kendig, and S. Tsai. Evaluation of corrosion behavior of coated metals with AC impedance measurements. *Corrosion*, 28(9):478–485, 1982.

[57] B.N. Popov, Mohammed A. Alwhaibi, and R.E. White. Organic coating solute saturation monitoring. *Journal of the Electrochemical Society*, 140(4):947–951, 1993.

[58] Miki Itoh, Masaru Ihara, Hiroshi Nishihara, and Kunitsugu Aramaki. Corrosion inhibition of cobalt in some acid solutions by bismuth(iii) chloride. *Journal of the Electrochemical Society*, 141(2):352–358, 1994.

[59] John R. Scully. Electrochemical impedance of organic-coated steel: Correlation of impedance parameters with long-term coating deterioration. *Journal of the Electrochemical Society*, 136:980–989, 1989.

[60] U. Außerlechner, W. Steiner, and P. Kasperkovitz. Calibration of vibrating sample magnetometers independent of reference samples. *Measurement Science and Technology*, 7:1574–1578, 1996.

[61] Henry Leidheiser Jr. *Corrosion Mechanisms*, volume 28 of *Chemical Industries*, chapter Coatings, pages 165–209. Marcel Dekker, New York, 1987.

[62] M. Piens and R. Verbist. Electrochemical values: Their significance when applied to a coated substrate. In H. Leidheiser Jr., editor, *Corrosion Control by Organic Coatings*, pages 32–37. NACE, Houston, TX, 1981.

[63] F. Mansfeld, M. Kendig, and S. Tsai. Evaluation of organic coating/metal systems by AC impedance techniques. In *Proceedings of the 8th International Congress on Metallic Corrosion*, volume 2, pages 1014–1020, Frankfurt am Main, Germany, 1981. International Corrosion Council, DECHEMA.

[64] S.S. Abd El Rehim, A.A. El Basosi, and M.M. Osman. The influence of halide ions on the corrosion and passivity of cobalt in an alkaline medium. *Journal of Electroanalytical Chemistry*, 348:99–106, 1993.

[65] D.H. Davies and G.T. Burstein. The electrochemical behavior of cobalt in bicarbonate and borate electrolytes. *Corrosion Science*, pages 973–987, 1980.

[66] A.A. Aksut. The corrosion behavior of cobalt and nickel in sulfuric acid solution containing propargylic acid. *Corrosion*, 40(8):418–420, 1984.

[67] N.S. McIntyre and M.G. Cook. X-ray photoelectron studies on some oxides and hydroxides of cobalt, nickel, and copper. *Analytical Chemistry*, 47(13):2208–2213, 1975.

[68] C. Chandler, J-B Ju, R. Atanasoski, and W.H. Smyrl. Corrosion and electrodissolution studies of cobalt and copper thin films with the quartz crystal microbalance and microelectrodes. *Corrosion*, 47(3):179–184, 1991.

[69] M. Piens, J. Hubrecht, and J. Vereecken. Electrochemical methods to determine the corrosion rate of coated metals. In *Proceedings of the 8th International Congress on Metallic Corrosion*, volume 2, pages 1021–1025, Frankfurt am Main, Germany, 1981. International Corrosion Council, DECHEMA.